RSC Pharmaceutics

ROYAL SOCIETY OF CHEMISTRY

PAPER

View Article Online
View Journal | View Issue

Cite this: *RSC Pharm.*, 2025, **2**, 772

Calcium phosphate reinforced chitosan–carrageenan scaffolds: characterization and *in vitro* assessment for wound healing†

Vinita Patole, *[a] Gaurav Kavitkar, [a] Ganesh Ingavle,[b] Isha Behere,[c] Ravindra Wavhale,[d] Abhishek Jha,[a] Sanjeevani Deshkar,[a] Avinash Sanap[e] and Pramod Sakpal[f]

Wound healing is a multifaceted and dynamic biological process, which traditional wound dressings often fail to adequately support, leading to prolonged healing times. It would be highly beneficial to develop wound dressings with the ability to support biological processes such as cell proliferation and angiogenesis and deliver the active agents required to restore intracellular activities to promote wound healing. The current work aimed at developing a polyelectrolyte complex of chitosan (CH) and an anionic polymer, condensed with calcium phosphate (CaP) powder to attain antibacterial and angiogenic potential, cell proliferation, appropriate swelling index, and enhanced wound healing. Polyelectrolyte complexes (PECs) were formulated using chitosan (CH), as a cationic polymer and pectin (PE), sodium alginate (SA), and carrageenan (CA), respectively, as an anionic polymer through a lyophilization process. PEC formation was confirmed by FTIR, XRD, and DSC by observing the changes in their vibrational frequencies, structures, and thermal properties. SEM revealed the porous structure of the scaffolds. From the prepared PEC scaffolds, chitosan–carrageenan (CH-CA) was selected for further studies based on the swelling index, porosity, and degradation studies. Following the production of CaP powder using a microwave-assisted synthesis method, the powder was characterized by FTIR, SEM, XRD, and energy dispersive X-ray (EDX) techniques before being loaded onto CH-CA scaffolds. The results demonstrated approximately 60.75% release of calcium ions (Ca^{++}) from the CH-CA scaffolds in PBS, pH 5.5, as analysed by atomic absorption spectroscopy (AAS) over 24 h. The scaffolds demonstrated a higher swelling index and exhibited antimicrobial activity against *E. coli* and *S. aureus*. The scaffolds were found to be hemocompatible and demonstrated angiogenic potential, evidenced by stimulating new blood vessel development in a chick yolk sac membrane assay. Cell proliferation studies demonstrated the cytocompatibility of the scaffolds, and improvement in the cell density of the L929 mouse fibroblast cell line was observed in a live/dead assay. In conclusion, the calcium-loaded CH-CA scaffolds demonstrated antimicrobial properties, increased angiogenesis, blood compatibility, and cell proliferation, indicating their potential as an appropriate wound dressing material.

Received 2nd October 2024,
Accepted 23rd April 2025

DOI: 10.1039/d4pm00284a

rsc.li/RSCPharma

[a]*Department of Pharmaceutics, Dr D. Y. Patil Institute of Pharmaceutical Sciences and Research, Pimpri, Pune 411018, India. E-mail: Vinita.patole@dypvp.edu.in; Tel: +9730388345*
[b]*Advanced Cell and Gene Therapy Manufacturing (GMP) Unit, NIHR Biomedical Research Centre Guy's and St Thomas' NHS Foundation Trust and King's College London, Clinical Research Facility, Guy's Hospital, London, SE1 9RT, UK*
[c]*Symbiosis Centre for Stem Cell Research (SCSCR) and Symbiosis School of Biological Sciences (SSBS), Symbiosis International (Deemed University), Pune 412115, India*
[d]*Department of Chemistry, Dr D. Y. Patil Institute of Pharmaceutical Sciences and Research, Pimpri, Pune 411018, India*
[e]*Regenerative Medicine Laboratory, Dr D.Y. Patil College and Hospital, Dr D.Y.Patil Vidyapeeth, Pimpri, Pune, India*
[f]*Department of Chemistry, Marathwada Mitra Mandal's College of Pharmacy, Pune 411033, India*

†Electronic supplementary information (ESI) available. See DOI: https://doi.org/10.1039/d4pm00284a

1. Introduction

A wound is defined as a disruption in the skin's or mucosa's epithelial lining, which may result in temporary or permanent damage. Wounds often occur because of various reasons such as physical trauma, cuts, burns, diseases or accidents.[1] In response to such an injury, the tissue regeneration process facilitates the repair of wounds, involving various types of cells, cytokines, and a stable supply of ions.[2] During the tissue regeneration process, a range of molecular and cellular events take place along with various physiological changes in the body.[3] Upon tissue injury, calcium ions are reported to play a significant role in regulating various signalling pathways, which affect the intracellular activities essential for wound

healing.[4] Studies have reported that extracellular calcium concentration rises post-injury and remains elevated during the proliferative and inflammatory stages. As both an extracellular signaling molecule and an intracellular secondary messenger, the calcium ion facilitates diverse cellular activities such as activation of immune cells, fibroblasts, and keratinocyte growth and differentiation, which play a significant role in wound closure and formation of new tissues.[5] Moreover, calcium is often referred to as clotting factor IV, which may trigger the intrinsic coagulation cascade, which aids in thrombin formation, thus assisting in blood clotting during the hemostatic phase through platelet plug formation.[6] Furthermore, it is reported to stimulate angiogenesis, a vital and an essential stage in wound healing.[7] It aids in the reconstruction of the extracellular matrix during the remodeling phase.[5] Phosphate, in addition to calcium ions, plays a crucial role in wound healing by supplying the metabolic energy required for diverse cellular processes.[8] Therefore, developing wound dressings that release calcium might be an effective strategy to promote wound healing.

Various types of natural and synthetic polymeric materials, as well as their combinations, can be used to develop wound dressings. Despite significant progress in the field of wound dressing materials, there is still more to be done to create dressings that can ensure optimal hydration, guard against infection, and be simple to apply.[9] Recently, there has been great interest in the use of natural polymers for wound dressing due to their biocompatibility and close resemblance to the extracellular matrix (ECM). Natural polymers can be readily accepted by the biological system without stimulating immunological reactions usually linked with synthetic polymers.[10]

Chitosan (CH) is an excellent cationic biopolymer widely used for to its wound healing potential, owing to its characteristics including biocompatibility, antimicrobial, hemostatic, and anti-inflammatory properties.[11,12] Despite all the benefits that CH offers, its limited mechanical strength, rapid degradation, and poor adhesion limit its use in the development of wound dressing scaffolds. Hence, developing PECs of CH with an oppositely charged anionic polymer is a strategy to overcome the limitations of CH. The electrostatic bonding within oppositely charged polymers is necessary for PEC formation. Studies have reported that CH-based PECs exhibited improved performance in enhancing wound closure. Yaşayan G *et al.* developed chitosan/pectin-based polyelectrolyte complex films encapsulating silver sulphadiazine for wound healing by a casting and solvent evaporation method, and they displayed improved properties in terms of durability and excellent wound healing properties.[13] Similarly, Alven S *et al.* also described chitosan-based scaffolds incorporated with silver nanoparticles as a wound dressing material. These scaffolds demonstrated superior antibacterial properties with good biocompatibility and low toxicity which are essential qualities of an ideal wound dressing material.[14]

The aim of the current study was to develop a PEC-based CH film using three anionic polymers: pectin (PE), carrageenan (CA), and sodium alginate (SA), which were selected based on a literature survey. PE is a heteropolysaccharide mainly composed of α (1–4) linked D-galacturonic acid residues. It is a polyanionic polymer extracted from citrus fruits and is known for its biocompatibility and excellent water absorption properties. Nordin NN *et al.* developed drug-free pectin hydrogel films at two different concentrations: 2.5% and 5%, using a solvent evaporation method for the treatment of thermal burn wounds. The 5% concentration film demonstrated superior antimicrobial activity and facilitated faster wound healing in streptozotocin-induced diabetic rats.[15]

CA is a sulfated polysaccharide reported for use in wound healing. It is a biocompatible angiogenic and haemostatic agent, with good water-absorbing ability, making it suitable for wound closure by absorbing wound exudates.[16] Ulagesan *et al.* formulated a κ-carrageenan-R-phycoerythrin hydrogel for wound healing application. This hydrogel exhibited excellent antioxidant and antimicrobial activities along with a microporous and interconnected structure and good biodegradability.[17]

SA is an anionic natural polymer obtained from brown algae. It is reported to be a non-toxic, biocompatible, readily available, inexpensive, and haemostatic polymer widely explored as a wound dressing material.[18] Ishfaq B *et al.* developed a sodium alginate-based hydrogel dressing incorporating an extract of Betula utilized for wound healing by a solvent casting method, and it exhibited optimal folding endurance, an appropriate thickness, and antioxidant and antimicrobial properties.[19]

Considering the benefits offered by CH as a cationic polymer, and pectin, carrageenan, and sodium alginate as anionic polymers, PEC-based films were developed by the lyophilisation technique. The formulation of PECs was confirmed by different analytical techniques such as FTIR, DSC, and XRD. Furthermore, the lyophilized PECs were loaded with synthesized CaP powder. Calcium phosphate powder was synthesized by a microwave-assisted method and characterized by various *in vitro* techniques. The calcium-loaded PEC scaffolds were evaluated in terms of swelling index, *in vitro* release, angiogenesis, hemocompatibility, antimicrobial activity, and *in vitro* cell proliferation. Thus, this study shows that the development of calcium-loaded PEC scaffolds is a promising approach for wound healing applications.

2. Materials and methods

2.1 Materials

Calcium hydroxide (99.8% purity, extra pure) was purchased from LOBA Chemie (Mumbai, India). *ortho*-Phosphoric acid (85% purity, AR grade) was purchased from LOBA Chemie (Mumbai, India). Chitosan (98% purity, 93% deacetylation, MW 190 000–310 000 Da, viscosity 300–1000 cps) was purchased from Research Lab Fine Chem Industries (Mumbai, India) and sodium alginate (91% purity, MW 12 000–40 000 Da, viscosity 30 cps) was purchased from LOBA Chemie (Mumbai, India). Pectin (extra pure, MW 30 000–100 000, vis-

cosity 400–800 cps) was purchased from LOBA Chemie (Mumbai, India). l-Carrageenan (MW 100, 000 Da, viscosity 14 mPa. s) was purchased from HIMEDIA (Mumbai, India). All of the chemicals used were of analytical quality.

2.2 Preparation of scaffolds by a polyelectrolyte complex method

The PEC-based scaffolds were prepared by dissolving anionic polymers CA, SA, and PE separately in distilled water at 2% w/v by constant stirring. CH was dissolved in acetate buffer (pH 4) at 2% w/v. Furthermore, the anionic polymer solutions were added dropwise to the cationic CH solution separately with constant stirring at 1000 rpm for 3 h to obtain a weight ratio of 1 : 1 for each cationic and anionic polymer. These mixtures were then poured into a silicone mould (1 × 1 cm^2) and kept for deep freezing for 24 h at −80 °C (Remi ULT-185). Following this, the samples were lyophilized (Martin Christ, Alpha 2–4 LSC, an der Untener Sose, Germany) under freezing conditions for 30 minutes, warmed up for 20 minutes, and subjected to a main drying process for 4 h under vacuum (0.0050 m bar) and a final drying process for 4 h (vacuum, 0.1000 m bar). The freezing cycles were repeated for 4 days to eliminate the moisture completely.[20] The dried scaffolds were carefully removed from the moulds and characterized using FTIR, XRD, DSC, and SEM.

2.3 Characterisation of PEC-based scaffolds

2.3.1 FTIR. The FTIR absorption spectra of CH, PE, SA, CA, and their PEC-based scaffolds CH-CA, CH-PE, and CH-SA were recorded using a Bruker Alpha-II spectrophotometer (Germany, Europe) with multiple-reflection ATR (attenuated total reflectance). Using a resolution of 4 cm^{-1}, scanning was performed across the range of 400–4000 cm^{-1}.[21] To achieve the best possible contact between the sample and the ATR crystal, the sample was placed on the surface of the ATR crystal and forced down with a swivel press. OPUS software was used for peak processing.

2.3.2 Surface morphology (SEM). The surface morphological studies of the PECs were conducted using field emission scanning electron microscopy (FESEM, FEI, Apreo LoVac). Samples weighing about 5 mg were coated with a 20 nm layer of platinum in order to make them electrically conductive. Furthermore, the samples were scanned in the FESEM chamber using an acceleration voltage of 20.00 kV and a vacuum pressure of 1.30 × 10^{-4} Pa. Photomicrographs were captured at various magnifications.[20]

2.3.3 XRD. The X-ray diffraction spectra of the polymers CH, PE, and SA, as well as the CH-CA, CH-PE, and CH-SA scaffolds, were recorded using an X-ray diffractometer (Rigaku Model ULTIMA IV) with Cu K 2α rays with an energy of 40 kV and a current of 40 mA. The samples were scanned at 2θ angles from 10° to 80°.[22]

2.3.4 Differential scanning calorimetry (DSC). The thermal analysis of the polymers CH, CA, SA, and PE, as well as their PECs, was performed using differential scanning calorimetry (Hitachi DSC7020, Tokyo, Japan). The sample (1 mg) was heated under a continuous 20 mL min^{-1} nitrogen flow rate and a 10 °C min^{-1} heating rate. Using a blank aluminium pan as a reference, the DSC thermograms were recorded in the temperature range of 30–300 °C.[23]

2.3.5 Swelling index and porosity studies. The swelling index of the PECs was calculated by immersing pre-weighed samples of CH-CA, CH-PE, and CH-SA in PBS (pH 7.4) for a period of 5 h. After 5 h, the samples were reisolated, and, with the help of fine paper, the extra water on the surface of the PEC was removed and dried completely.[24] The dried scaffolds were weighed again, and the swelling index was calculated using the following formula:

$$\text{Swelling ratio} = (W_f - W_i)/W_i \times 100 \quad (1)$$

where W_f is the weight after 5 h and W_i is the initial weight of scaffolds.

Porosity studies were performed on each PEC scaffold to assess their effectiveness in wound healing applications. Initially, the dry weight of each PEC was recorded using an analytical balance. The PECs were then submerged in 100% ethanol in a graduated cylinder, ensuring full immersion, and soaked for 24 h at room temperature to allow thorough penetration of ethanol into the pores of the PECs. After complete soaking, the PECs were carefully removed and blotted gently to remove excess ethanol without compressing their structure and weighed again.[25]

The %porosity of PECs was determined by using the following formula:

$$\%\text{porosity} = ((W_f - W_i)/\rho_{ethanol}/V) \times 100 \quad (2)$$

where W_f and W_i are the weights before and after immersion in alcohol. The volume of alcohol is denoted as V, and the density of ethanol is denoted as ρ.

2.3.6 Degradation studies. Degradation studies were carried out on each PEC-based scaffold using the ninhydrin reagent method to evaluate their stability and degradation profile. Each PEC was submerged in a buffer solution (pH 7.4) to simulate physiological conditions. At respective time intervals, 1 mL sample was withdrawn from the solution. Fresh buffer was added to the withdrawn volume to maintain the sink condition. To 1 mL of this withdrawn sample, an equivalent volume of 8% ninhydrin reagent was added. The mixture was then heated at 80 °C for 15 min in order to facilitate the reaction between ninhydrin and the degradation products, typically the amino acids released from the PEC. After heating, the absorbance of the resulting solution was measured at 570 nm using a UV-visible spectrophotometer.[26]

2.4 Synthesis of CaP powder

The CaP powder was synthesized by a simple co-precipitation method using microwave-assisted synthesis. Initially, solutions of 0.45 M H_3PO_4 and 0.75 M $Ca(OH)_2$ were prepared. Subsequently the 0.45 M H_3PO_4 aqueous solution was added to the 0.75 M $Ca(OH)_2$ aqueous suspension under continuous stirring conditions at room temperature. Then, the resultant

reaction mixture was subjected to microwave irradiation at 850 W for 11 minutes in a microwave synthesizer (Catalyst, CATA 2R, India). The resulting white paste was dried in an oven to obtain a dry powder. The CaP powder was formed with a constant Ca/P molar ratio of 1.5.[27] The synthesized Ca phosphate powder was then subjected to different characterization techniques, including FTIR, SEM, DSC, XRD, SEM, and EDX. The reaction for the synthesis of calcium phosphate is outlined below:

$$3H_3PO_4 + 2Ca(OH)_2 \rightarrow Ca_3(PO_4)_2 + 6H_2O. \quad (3)$$

2.4.1 Characterization of CaP powder. The IR absorption spectra of the CaP powder were recorded using an FTIR spectrophotometer (Shimadzu, 8400S, Japan) across the range of 400–4000 cm^{-1}. Using an X-ray diffractometer (Rigaku ULTIMA IV) and Cu K 2α rays with an energy of 40 kV and a current of 40 mA, the X-ray diffraction analysis was performed. The samples were scanned at 2θ angles from 5° to 80°. The surface morphology was studied using FESEM (FEI, Apreo LoVac, USA) images. Energy-dispersive X-ray spectroscopy (EDX) of the synthesized calcium phosphate was carried out to determine the elemental composition. EDX analysis was performed using an Oxford Instruments X-Max 80 EDX detector with SEM. Samples were prepared by placing them on carbon-coated copper grids, and then the system was operated at an accelerating voltage of 20 kV and a working distance of 10 mm. Then, EDX spectra were taken.[28]

2.5 Calcium loading on the scaffolds and their *in vitro* characterization

A dispersion of calcium phosphate powder and the surfactant sodium cholate (0.2 wt%) was initially prepared in distilled water. After that, CH-CA scaffolds were immersed in the calcium phosphate dispersion (1 wt%) for 1 h at 10 °C. The scaffolds were rinsed in 70% ethanol and freeze-dried for 24 h.[29] The obtained scaffolds were then characterized using FTIR, XRD, DSC, and SEM analysis using the same procedures as described in the preceding section.

2.5.1 *In vitro* release study of Ca^{2+} ions. *In vitro*, Ca^{2+} ions released from the calcium-loaded CA scaffold were studied using phosphate buffer solution (PBS buffer) (pH 7.4). Approximately 100 mg of calcium-loaded CH-CA scaffold was placed in 100 ml buffer solution, followed by shaking continuously at 37 °C for 6 h. 1 mL sample was taken out at specific time intervals, and sink conditions were maintained. This 1 mL sample was diluted with a mixture of 6 M HNO_3 and water to obtain a final volume of 10 mL and the pH was maintained below 2. The release of Ca^{2+} ions was detected using an atomic absorption spectrophotometer (AAS) (PerkinElmer, USA PinAAcle 500) at wavelengths of 185 to 900 nm.[30]

2.5.2 Protein adsorption studies. Protein adsorption studies are highly significant for wound healing as they determine the interaction of various proteins with the surface of scaffolds. In the wound environment, various proteins are present which facilitate blood clotting and aid in the wound healing process. The protein adsorption behaviour of CH-CA scaffolds and calcium-loaded CH-CA scaffolds was studied using bovine serum albumin (BSA) as a reference protein by the batch contact method as described by Golafshan *et al.* Initially, 0.2 wt% solution of BSA was prepared in PBS (pH 7.4). Consequently, both the scaffolds were immersed in 20 mL of the prepared BSA solution and continuously agitated for 1 h at 37 °C. The scaffolds were removed and weighed. The absorbance of the residual BSA solution was recorded using a UV spectrophotometer at 280 nm.[31] The amount of BSA adsorbed on the surface of both scaffolds was estimated separately using the following formula:

$$\text{Amount of BSA adsorbed (mg g}^{-1}) = ((C_a - C_b)/W) \times V \quad (4)$$

C_a is the initial and C_b is the final concentration (mg mL^{-1}) before and after adsorption. W is the weight of the scaffolds after 1 h (g) and V is the volume of the BSA solution (mL).

2.5.3 *In vitro* hemolysis studies. Hemolysis potency determines the hematological stability of the scaffolds as they can directly interact with the blood. In this study, fresh blood samples were withdrawn from Wistar rats through the retro-orbital route and collected in a heparinized tube. These blood samples were centrifuged at 3000 rpm for 15 min for isolation of the erythrocytes (RBCs). The supernatant was discarded, and the RBCs were washed three times with PBS (pH 7.4). Subsequently, the erythrocytes were dispersed in PBS (pH 7.4) to form an erythrocyte suspension. From the resulting suspension, 50 μL of suspension was added to various concentrations (0.08, 0.2, 0.4, 0.6, 0.8, 1.0, and 1.2 mg mL^{-1}) of both the scaffolds, *i.e.*, CH-CA and calcium-loaded CH-CA scaffolds. A blood sample that was only mixed with distilled water was used as the negative control. All the samples were incubated for 1 h in the dark and then centrifuged at 3000 rpm for 20 min. The absorbance of the resulting supernatant was recorded on a UV-spectrophotometer at 548 nm and %hemolysis was determined using the following formula:

$$\%\text{hemolysis} = ((D_a - D_n)/(D_p - D_n)) \times 100 \quad (5)$$

where D_a is the absorbance of the sample, D_n is the absorbance of normal saline, and D_p is the absorbance of the distilled water, respectively.

2.5.4 *In vitro* antimicrobial activity. Antibacterial activities of the formulated CH-CA scaffolds and calcium-loaded CH-CA scaffolds against *E. coli* (Gram-negative bacteria) and *S. aureus* (Gram-positive) bacteria were evaluated by measuring the zone of inhibition. Initially, bacterial suspensions of *S. aureus* and *E. coli* were prepared by suspending small colonies of both the micro-organisms in 10 mL of PBS with the turbidity being maintained at 0.5 in accordance with the McFarland standard. Then, 100 μL of each bacterial suspension was spread uniformly over sterile agar plates with the help of a sterile glass spreader.[32] Then, CH-CA scaffolds and calcium-loaded CH-CA scaffolds of the size 1 × 1 cm^2 were placed on the prepared agar plates and kept at 37 °C for 48 h. The resulting zone of inhibition was measured after 48 h.

2.5.5 *In ovo* angiogenesis study by a chick yolk sac membrane (YSM) assay. The YSM model is widely used as an effective *in vivo* model for screening the angiogenic potential of scaffolds.[33] The angiogenesis activity was analyzed as per the method described by Patole *et al.* Eggs (day 0) were collected from Venkateshwara Hatcheries Pvt. Ltd, Pune (India). After washing with ethanol, the eggs were incubated in a humidified incubator and maintained at 37 °C for 48 h for incubation. Following this, a tiny incision was made at the narrow end of the egg, and 2–3 mL of albumin was taken out with a micropipette. This created a free space between the shell and the embryonic structure. Subsequently, CH-CA scaffolds and calcium-loaded CH-CA scaffolds were put on the yolk sac membrane. The eggs were covered with cellophane tape and reincubated for 48 h. The tape was removed, and blood vessels were photographed using a digital camera.[34,35]

2.5.6 MTT assay (cell cytotoxicity assay). An MTT test was carried out to identify the cytotoxicity of calcium-loaded CH-CA scaffolds on the cell viability of L929 mouse dermal fibroblast cells. Briefly, calcium-loaded CH-CA scaffolds (5 × 5 mm^2) were sterilized using 70% ethanol for 15 minutes and then washed three times with PBS solution (pH 7.4) and subjected to UV sterilization in a laminar flow hood under UV light. The scaffolds were then submerged in DMEM (Dulbecco's modified Eagle's medium) supplemented with 10% fetal bovine serum (FBS) and maintained at 37 °C for 24 hours in a CO_2 incubator. A 96-well plate containing 5×10^3 cells (L929 Mouse fibroblast cells) was seeded with 100 μL of DMEM with 10% FBS and incubated overnight. After a period of 24 h, 100 μL of the leached medium from the scaffold was added to every well and incubated for another 24 h. After discarding the medium, the cells were then treated for four hours with 100 μL of serum-free DMEM containing 10 μL of MTT (5 mg mL^{-1}). Then, formazan crystals were dissolved in each well by adding 100 μL of DMSO. The absorbance was recorded with a microplate reader at a wavelength of 570 nm, whereas the non-treated cells were considered 100% viable.[36]

2.5.7 Live/dead assay. A live/dead assay was performed using L929 mouse dermal fibroblast cells grown in DMEM containing 10% FBS. Initially, the calcium-loaded CH-CA scaffolds and a marketed sample (Bactigras) were sterilized *via* exposure to UV light for 30 minutes. Subsequently, the cells were seeded at a density of 2×10^4 (cells/cm^2) onto the surface of both the scaffolds and incubated for 48 h at 37 °C with 5% CO_2 to enable cell attachment and growth. The viability of the cells on the surface of calcium-loaded CH-CA scaffolds and the marketed sample Bactigras was assessed using a LIVE/DEAD™ cell viability/cytotoxicity kit (Invitrogen, USA). Following incubation, both the scaffolds were removed, gently washed with PBS, and incubated with the live/dead assay solution for 15 minutes at room temperature, away from sunlight. The scaffolds were gently placed on clean glass slides, and the stained cells were observed using an immunofluorescence microscope. The images were captured across multiple fields of view and analysed using image analysis software to determine the percentage of living and dead cells.

3. Results and discussion

3.1 FTIR of scaffolds

FTIR analyses allow for identifying specific functional groups within the complexes and assessing the interaction between the polymers during the formation of PECs (Fig. 1). The FTIR spectra of CH displayed symmetrical bending vibration at 3359 cm^{-1}, which may be present due to the overlapping of OH and NH_2 groups. The amine group exhibited an absorption band at 1590 cm^{-1}, whereas the carbonyl group displayed a characteristic band at 1646.97 cm^{-1}. The FTIR spectra of CA displayed an OH group at 3269.24 cm^{-1}, an aliphatic CH group

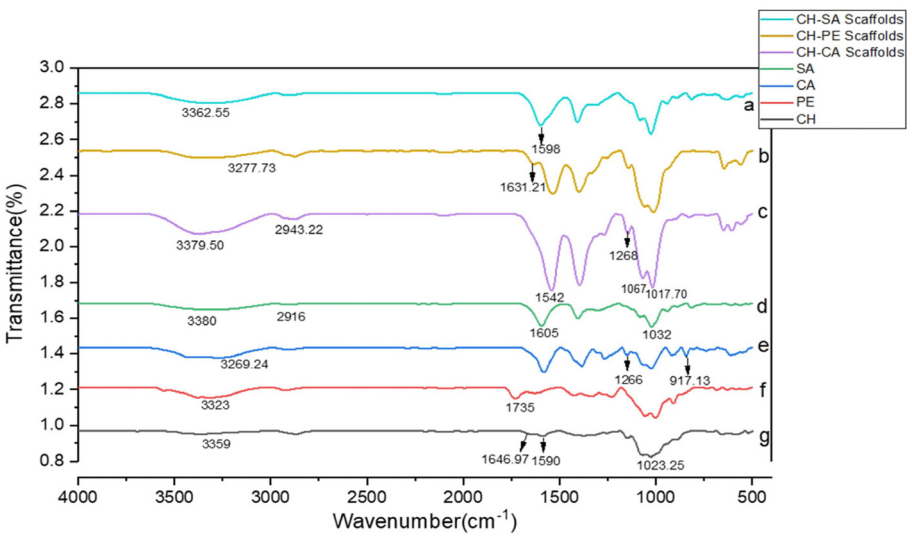

Fig. 1 FTIR of (a) CH-SA scaffolds, (b) CH-PE scaffolds, (c) CH-CA scaffolds, (d) SA, (e) CA, (f) PE, and (g) CH.

shows stretching at 2919.48 cm^{-1}, and the broad bands at 1266 cm^{-1} and 1303 cm^{-1} assigned to S=O may be due to the presence of the SO^3 group. The peak at 917.13 cm^{-1} was assigned to the 3,6-anhydrogalactose unit. In the case of PE, the OH group is observed at 3323 cm^{-1}. The carbonyl group exhibited a band at 1735 cm^{-1}, and the aliphatic CH group displayed an absorption band at 2362.80 cm^{-1}. The FTIR spectra of SA displayed O–H stretching at 3380 cm^{-1}, aliphatic C–H stretching at 2916 cm^{-1}, a carbonyl group band at 1605 cm^{-1}, and C–O stretching at 1032 cm^{-1}.[20] The formation of a polyelectrolyte complex is a result of electrostatic interaction between the anionic and cationic polymers. During the development of PECs, the FTIR spectra show several modifications, such as the appearance of additional absorption bands, shifting of wave numbers, and band broadening. The OH stretching band in chitosan shifts from 3359 cm^{-1} to 3379 cm^{-1} in the CH-CA complex, indicating new hydrogen bonding between chitosan's hydroxyl groups and carrageenan's sulphate groups. This alteration reflects changing electron density and bond strength caused by electrostatic and hydrogen-bonding interactions that occur during polyelectrolyte complex (PEC) formation. The disappearance of the amine band at 1590 cm^{-1} and the carbonyl group band at 1646.97 cm^{-1} in chitosan (CH) is a crucial observation. The new band at 1542 cm^{-1} that emerges in the CH-CA complex can be attributed to the interaction between the amine group of chitosan and the sulfate group of carrageenan. This interaction likely leads to a shift in the vibrational frequency of the N–H bending and C=O stretching, indicating the formation of electrostatic interactions that affect the molecular environment of the respective groups. This band shift is consistent with previously reported studies, such as those by Deshkar *et al.*,[20] who also observed similar changes in PECs, further supporting the presence of an electrostatic interaction between the amino group of chitosan and the sulfate group of carrageenan. The CH-CA complex exhibits a weak absorption band at 1017.3 cm^{-1}, which is due to the anhydrogalactose unit. This shows that carrageenan's structural units play a role in the complexation process, most likely due to the formation of a network that connects both polymer chains.[37] The FTIR spectra of CH-PE displayed an absorption band for the O–H group at 3277.73 cm^{-1}, and the spectra demonstrated a single absorption band at 1631.21 cm^{-1}, masking the CH amide as well as the carbonyl group in pectin. The results indicated an interaction between the amino group of CH and the carbonyl group of PE.[38] In CH-SA spectra, the peak for the O–H group was observed at 3196 cm^{-1}, which in the spectrum of SA was shifted to 3362 cm^{-1}. A single absorption band was observed at 1598 cm^{-1} masking the amide bands of CH, which indicates the formation of amide bonds and relates to the interaction within the carbonyl group of SA and the amino group of CH.[39] A notable reduction in the intensity of the sulfate group (S=O) peaks at 1266 cm^{-1} and 1303 cm^{-1} in the CH-CA spectrum suggests that some of the sulfate groups in carrageenan are involved in the interaction with the cationic amino groups of chitosan. This reduction in intensity is indicative of a successful complexation process, where some of the sulfate groups are neutralized by electrostatic interactions with the positively charged amine groups of chitosan.

3.2 XRD of scaffolds

An XRD study was carried out to study the solid state of the polymers as well as their PECs (Fig. 2). XRD studies help to investigate the effect of interactions between the different polymers on the crystalline structure during the formation of PECs. The XRD spectrum of SA displayed two broad peaks at 2θ = 13.54° and 2θ = 21.22° revealing the semi-crystalline nature of sodium alginate. Similar results were reported by Hezma *et al.*[40] PE displayed various peaks at 2θ = 8.4°, 12°, 13°, 18.72°, 19.46°, and 24.52°.[41] The XRD spectrum of carrageenan displayed peaks at 2θ = 12°, 17.70°, and 28.55°.[42] In the case of CH-SA, the XRD spectra displayed notable broad peaks at 2θ = 14.64°, 18.32°, and 22.72°, revealing its amorphous nature. Weakening of individual polymer bonds was observed, indicating an interaction between the polymers to form PECs.[43]

The broad peaks in the XRD patterns of CH-PE (2θ = 13.54° and 20.36°) and CH-CA (2θ = 11.83° and 18.48°) scaffolds result from the disruption of the crystalline structure of the individual polymers due to strong electrostatic and hydrogen-bonding interactions during polyelectrolyte complex (PEC) formation. These interactions weaken the individual polymer bonds, as evidenced by the disappearance of distinct peaks originally present in PE and CA, and lead to the formation of a more amorphous structure.

The broad nature of the peaks can be attributed to the heterogeneous distribution of polymer chains within the complex matrix, resulting in a reduced long-range order and a transition from a semi-crystalline or crystalline state to an amorphous state. This observation aligns with previous reports, such as those by Hezma *et al.*[40] where similar broadening was observed upon complexation of polymers.

3.3 DSC of scaffolds

A DSC study was performed to investigate the thermal changes occurring in the polymeric structure during the formation of PECs (Fig. 3). CH showed a broad endothermic peak at 119.9 °C which may be associated with the evaporation of bound water. It also exhibited an exothermic peak at 255.9 °C, associated with the thermal degradation of the polymer, which may be related to the breakdown of polymeric chains.[20,44]

CA displayed a small endothermic peak at around 80 °C due to the loss of bound water molecules from the polymer. The sharp endothermic peak at 167.7 °C indicated the melting temperature of CA.[45] PE displayed one broad peak near 90 °C, indicating the evaporation of bound water molecules from the polymer chains. The sharp endothermic peak at 185.2 °C indicated the melting point of pectin, and the peak at 210.9 °C indicated the degradation of the polymer. SA displayed an endothermic peak at 97.1 °C, which was attributed to the loss of bound water molecules due to the presence of hydrophilic groups, and an exothermic peak around 255.9 °C, which may

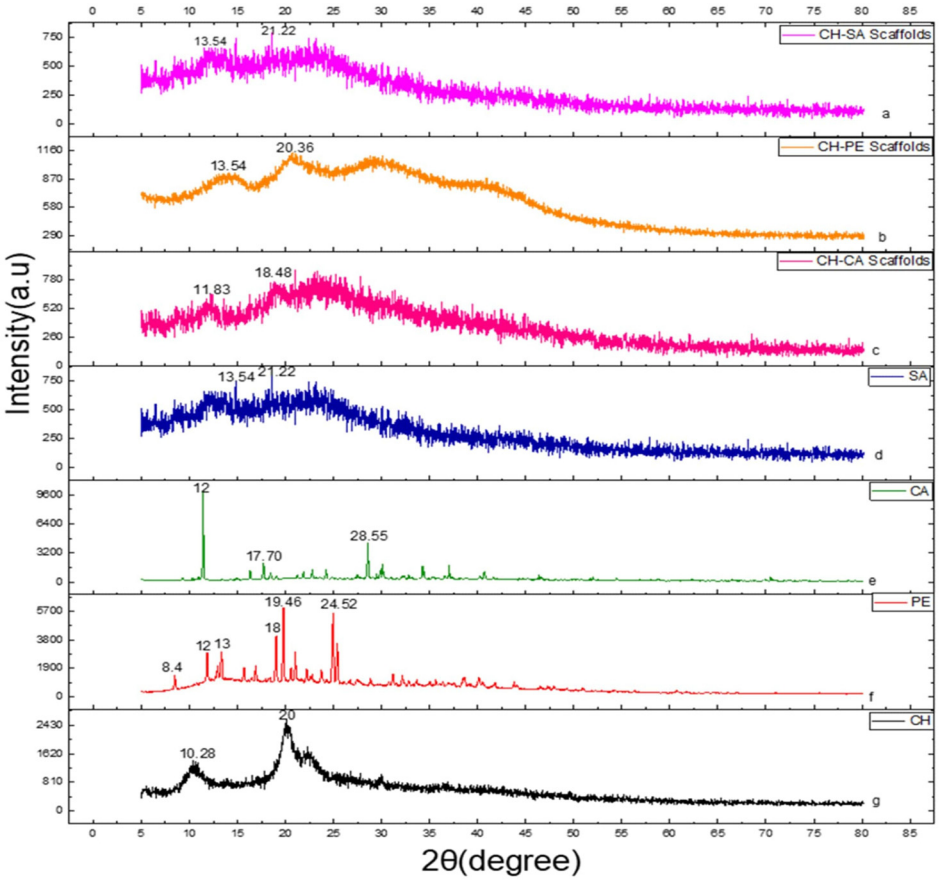

Fig. 2 XRD of (a) CH-SA scaffolds, (b) CH-PE scaffolds, (c) CH-CA scaffolds, (d) SA, (e) CA, (f) PE, and (g) CH.

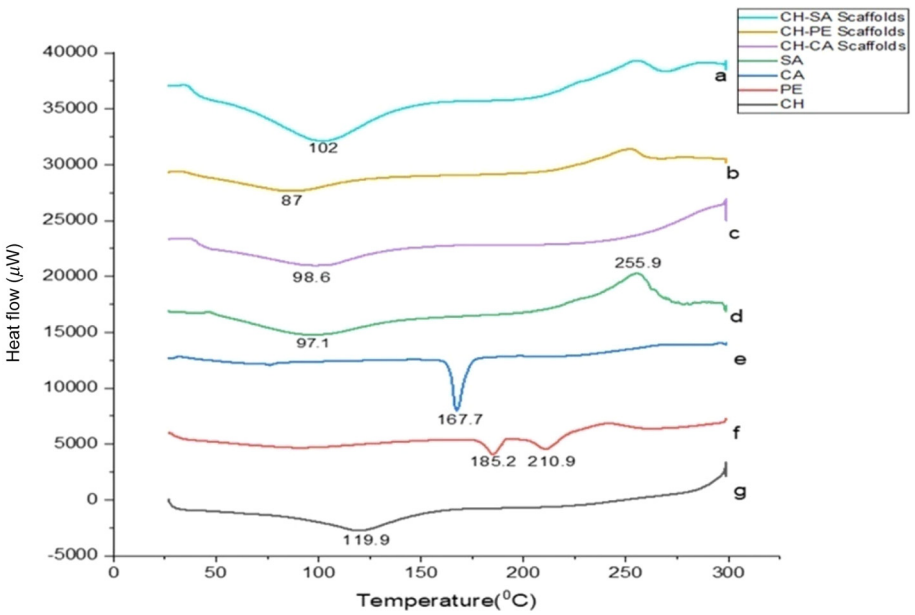

Fig. 3 DSC of (a) CH-SA scaffolds, (b) CH-PE scaffolds, (c) CH-CA scaffolds, (d) SA, (e) CA, (f) PE, and (g) CH.

be due to the thermal decomposition of the polymeric chains.[46]

The formation of PECs involves the creation of electrostatic or weak van der Waals interactions between the polymers. When two polymers interact to form a PEC, the resulting DSC spectra of the complex often show a shift or disappearance of distinct thermal transitions of the individual polymer. The reason for this is the change in the mobility and the arrangement of the polymeric chains which may result in alteration in the melting endotherm due to the loss of order within the material. The appearance of new thermal transitions or the broadening or merging of existing peaks in the DSC thermogram can be further used to observe this loss of order and arrangement of polymer chains within the material.

The DSC thermogram of CH-SA displayed an endothermic peak at 102 °C which was attributed to the loss of water molecules from the polymer chains. The disappearance of the exothermic peak of SA indicated the disruption of interpolymer interactions, thereby confirming the involvement of SA polymer chains in the formation of PECs.[20,47] In the case of the CH-PE PEC, a broad peak at 87 °C was observed, which was attributed to the evaporation or loss of water. The peak at 185.2 °C, corresponding to the melting of pectin, disappeared, which indicated the PEC formation.[48] The DSC thermogram of the CH-CA PEC displayed a peak at 98.6 °C, owing to the evaporation of water molecules from the polymer chains. A broad endothermic peak was observed from 260 °C onwards. The peak at 167.7 °C corresponding to the melting of CA disappeared, which shows the formation of electrostatic bonding between CA and CH.

3.4 Porous morphology of scaffolds

The porous surface morphology assessments of the lyophilized PECs were carried out using FESEM analysis (Fig. 4). The surface morphology can be better correlated with the porosity and swelling index of the PECs. The porosity and swelling index play significant roles in wound closure. The images were captured at low magnification because this level of magnification reveals important surface features, such as porosity and roughness, more clearly. The differences in scaffold porosity and surface roughness arise from the intrinsic properties of the individual polymers and their interactions during polyelectrolyte complex (PEC) formation. The compact and dense morphology of the CH-PE PEC, with less porosity, may be attributed to higher electrostatic interactions between chitosan and poly(ethylene glycol), resulting in a densely packed structure with reduced pore formation (Fig. 4A). The uniform and interconnected porous structure with larger pores of the CH-SA PEC scaffold results from weaker interactions and the high water solubility of sodium alginate, which facilitates greater phase separation during lyophilization, contributing to higher porosity and swelling (Fig. 4B). The smaller projections and small pores observed in the CH-CA PEC scaffold are likely due to moderate electrostatic interactions between chitosan and carrageenan, resulting in a semi-crystalline matrix with limited pore formation (Fig. 4C).[49]

3.5 Swelling index

The swelling index refers to the extent to which a PEC or scaffold material can absorb fluid and swell when exposed to the wound exudate. The swelling index of the scaffolds is shown in Fig. 5A. It measures the ability of the scaffold to absorb and retain moisture required for optimal wound healing. Ideally, the swelling index of the scaffolds used for wound healing should balance fluid absorption and retention, while also maintaining structural integrity and a moist environment conducive to healing.[50] The CH-SA PEC exhibited the highest swelling index, around 398.74 ± 2.34, which could be due to the highly porous structure of the CH-SA PEC, thereby allowing a larger volume of fluid to accumulate within its internal structure. Additionally, the pores were uniformly connected, which further ensures a uniform fluid distribution within the material. The FESEM images of CH-SA clearly indicated a uniformly interconnected porous structure. The CH-CA PEC showed a swelling index of 223.28 ± 2.92, whereas CH-PE exhibited a swelling index of 143 ± 2.6. The reason for this could be the presence of abundant carboxyl groups in pectin, which can readily interact with the amino groups in chitosan through strong electrostatic interactions, forming dense networks that result in a compact and less porous structure, which is evident from the FESEM images of the CH-PE PEC. The close packing of the polymers restricted the entry of water into the polymeric network resulting in a lower swelling index. A higher swelling index of the PEC may lead to various side effects such as delayed healing, mechanical instability, or

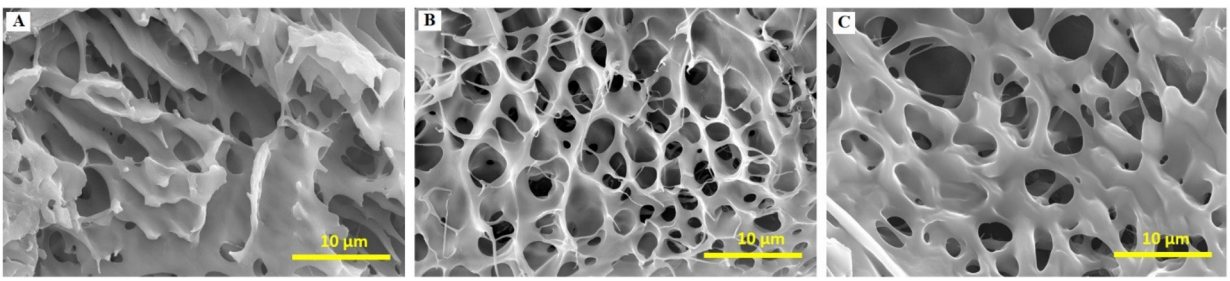

Fig. 4 Representative SEM micrographs showing the surface morphology of (A) CH-PE, (B) CH-SA, and (C) CH-CA scaffolds.

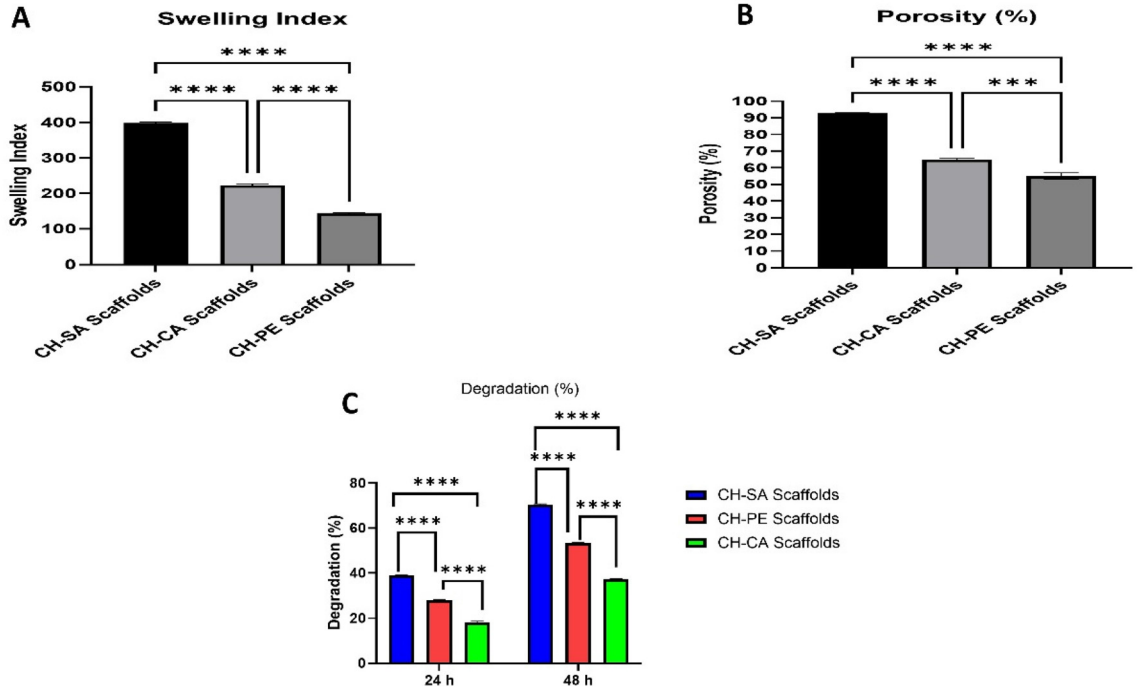

Fig. 5 (A) Swelling index of scaffolds, (B) porosity studies of scaffolds, and (C) degradation studies of scaffolds. Data are shown as mean ± SD (****p < 0.0001, ***p < 0.001).

leakage, leading to the pooling of exudate around the wound site. On the other hand, a lower swelling index of PECs may cause discomfort in the wound area. Additionally, an inadequate level of moisture may potentially hinder the cellular activities required for tissue regeneration. The results from the swelling studies indicated that the swelling index of CH-CA is within the optimal range, ensuring the maintenance of a moist wound environment without excessive swelling or loss of mechanical stability.[51]

3.6 Percentage and porosity studies

The porosity of a scaffold is crucial in wound healing applications as it plays a critical role in fluid absorption and tissue integration. The porosity of the scaffolds determines their ability to absorb and retain fluids.[52] The porosity of the scaffolds was measured using the liquid displacement method by soaking the scaffolds in ethanol, and the volume of ethanol absorbed corresponds to the pore size of the scaffold. The CH-SA scaffolds demonstrated the highest porosity, approximately 92.7 ± 1.30%, while the CH-CA scaffold showed a porosity of 64.91 ± 0.61%. In contrast, the CH-PE scaffolds exhibited a porosity of 54.93 ± 1.91% (Fig. 5B). As per Nosrati *et al.*, scaffolds with a 60–90% porosity value are suitable for wound healing as they may provide a sufficient void space for oxygen nutrient exchange and cellular activity. On the other hand, excessive porosity may affect mechanical strength due to higher fluid absorption and excessive swelling, which in turn might affect the degradation rate of the scaffold.[53]

3.7 Degradation studies

The degradation rate of PECs should be controlled and must be synchronized with the tissue regeneration process. The degradation rate of the scaffolds is shown in Fig. 5C. Ideally, a PEC-based scaffold for wound healing should degrade at a rate that provides support during the early stages of healing but gradually break down as new tissue forms and matures.[54] A controlled degradation rate of the scaffold ensures that it does not interfere with the healing process and delivers the biomolecules contained within the scaffold structure at the wound site. The rate of degradation of the scaffolds was studied using the method described by Sharma using the ninhydrin reagent.[26] According to this method, when the scaffold made of chitosan degrades, free molecules of chitosan are released. These molecules contain an amine group, which reacts with the ninhydrin reagent and forms a purple color complex that can be quantified using a UV spectrophotometer. The rate of degradation was measured at intervals of 24 and 48 h. In the case of CH SA scaffolds, the rate of degradation was approximately 38.95 ± 0.95% at 24 h and 70.46 ± 0.24% at 48 h. This is likely due to the higher porosity, which leads to faster degradation because of the increased surface area exposed to the wound fluid and, ultimately, a higher swelling index of the PEC. The higher porosity and swelling index might have resulted in lower mechanical strength of the PEC, thereby increasing the rate of degradation. The CH-PE scaffolds exhibited a degradation rate of 27.95 ± 0.16% at 24 h and 53.45 ± 0.12% at 48 h. In contrast, the degradation rate of CH-CA scaffolds was approximately 18.31 ± 0.32% at 24 h and

27.27 ± 0.18% at 48 h. CA has a higher molecular weight than pectin and sodium alginate. High molecular weight polymers, with their long polymeric chains, can provide greater resistance to degradation. Additionally, higher molecular weight polymers often have strong intermolecular interactions and tight packing, which might further hinder the degradation of the polymer chains.[55] Studies report that after injury, the natural tissue regeneration process generally begins within the first 24 to 48 hours. During this tissue regeneration process, the scaffold should degrade at a controlled rate, providing structural support and a conducive environment for cell growth and tissue formation, and then gradually degrade with the formation of new tissue. The results of the degradation studies indicate that the CH-CA scaffold exhibited a controlled rate of degradation.

Conclusively, the CH-CA PEC-based scaffold demonstrated an optimal swelling index required to maintain an environment conducive to wound healing, balanced porosity to enable adequate fluid absorption and sufficient mechanical strength. Additionally, it demonstrated a controlled degradation rate necessary for the scaffold to remain at the wound site for optimal tissue repair. Hence, the CH-CA PEC was further used to load Ca phosphate powder and was evaluated using different *in vitro* characterization studies to explore its wound healing potential.

3.8. Characterization of CaP synthesis

CaP powders, available commercially in various grades and compositions, are prone to absorb moisture during prolonged storage or when exposed to environmental conditions like humidity. This moisture uptake can lead to hydrolysis, which can further affect the stability of the powders. To alleviate these effects, synthesizing fresh calcium phosphate could be a beneficial approach.[56] Conventional methods for synthesizing CaP, such as hydrolysis, wet and dry hydrothermal techniques, solid-state synthesis, and sol–gel synthesis, come with limitations such as being tedious, time-consuming and having stability issues.[57] To overcome these problems, CaP can be synthesized using the microwave-assisted synthesis method, which is considered as one of the green synthesis routes. This method offers various advantages like better yield, high purity, uniform heating, and shorter reaction times.[58]

The FTIR spectrum of the synthesized CaP powder is shown in Fig. 6A, which reveals the presence of a hydroxyl (OH^-) bond stretch around 674 cm^{-1}. The peak at 465 cm^{-1} was attributed to υ_2 PO_4^{3-} stretching. The sharp peak obtained at 1030 cm^{-1} corresponds to υ_3 P–O asymmetric stretching. The peak at 564 cm^{-1} was assigned to υ_4 PO_4^{3-} bending. The small peak at 870 cm^{-1} was assigned to the presence of the HPO_4^{2-} band.[59] The XRD spectrum of the synthesized calcium phosphate powder displayed a broad peak at 2θ = 32°, which was identified as amorphous calcium phosphate. The results obtained were similar to those of the study conducted by Indurkar *et al.*[60]

The FESEM images of the synthesized calcium phosphate powder exhibited an irregular, uneven, and rough surface in the form of agglomerates (Fig. 6D).[61] In the EDX spectra of the synthesized CaP, four peaks are clearly visible (Fig. 6C), which are present between 0.1 keV and 1.50 keV. The synthesized calcium phosphate contained 73% of O, 13% of P, 13.4% of Ca, and 0.1% of C. The EDX spectra clearly showed the presence of calcium, phosphorus, and oxygen, which are the major

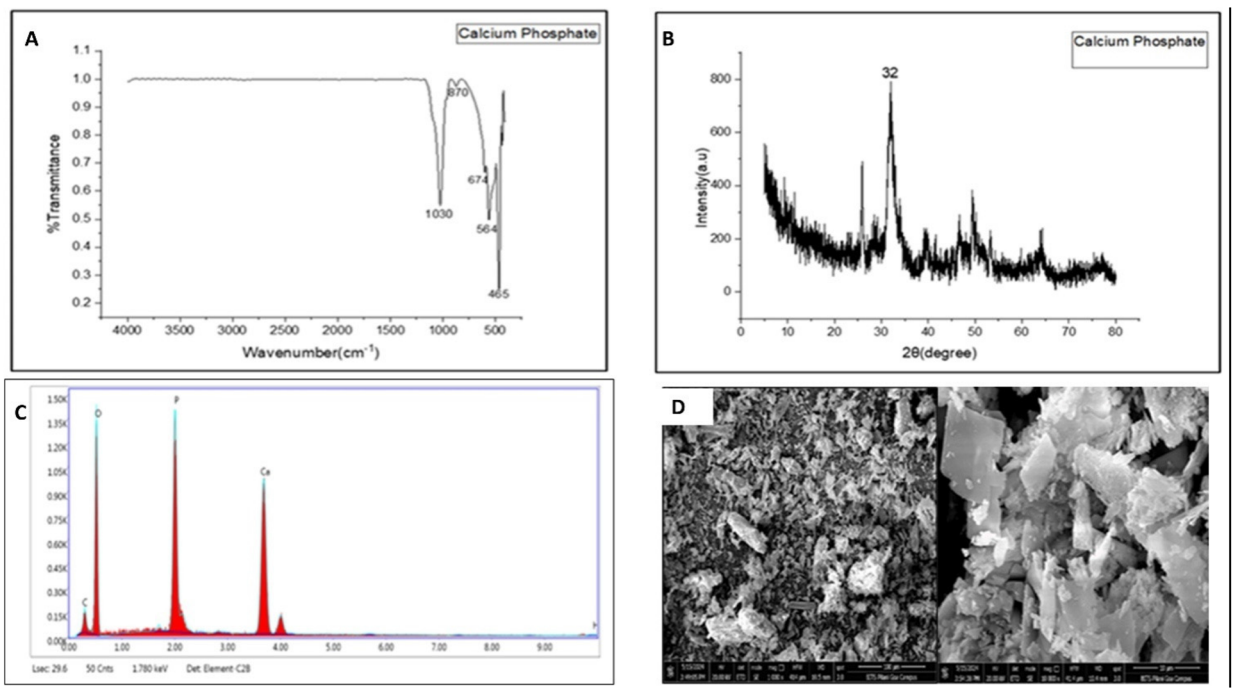

Fig. 6 (A) FTIR, (B) XRD, (C) EDX, and (D) SEM images of the synthesized CaP.

elements present in CaP, indicating the successful synthesis of CaP.[30]

3.9. Characterization of calcium-loaded CH-CA scaffolds

FTIR of CH-CA scaffolds revealed peaks at 3379 cm^{-1}, 2943 cm^{-1}, 1266 cm^{-1}, and 1026 cm^{-1} (Fig. 7A), which can be clearly seen. Calcium-loaded CH-CA scaffolds showed almost the same peaks as those of the CH-CA scaffolds. Additionally, a peak at 564 cm^{-1} is present due to the PO_4^{3-} bending of the calcium phosphate, and a peak at 870 cm^{-1} is present due to the HPO_4^{2-} band. These peaks show the successful incorporation of calcium phosphate in the scaffolds. The DSC thermogram of calcium-loaded CH-CA scaffolds showed one endothermic peak at 78.9 °C and one broad exothermic peak near 300 C. The endothermic peak at 78.9 °C may be due to evaporation of bound water.[62] The exothermic peak beyond 300 °C may be due to polymer degradation of CH.[63] The XRD of calcium-loaded CH-CA scaffolds exhibits two broad peaks at 2θ = 13.08° and 2θ = 20.56° indicating their amorphous nature.[62] The FESEM images of calcium-loaded CH-CA scaffolds showed the deposition of calcium phosphate particles all over the surface of the scaffolds (Fig. 7D). In another image, highly agglomerated particles of calcium phosphate are present, which may be due to the freeze-drying process.[29]

3.10. *In vitro* Ca^{2+} ion release studies

In vitro calcium ion release studies were performed in PBS (pH 5.5), showing significant and controlled release of calcium ions from scaffolds over 24 hours. The cumulative percentage of calcium released, as analyzed by AAS, was 60.75% at the end of 24 h (Fig. 8). The release of calcium was determined in PBS (pH 5.5) because the acidic microenvironment in the wound area is caused by temporary acidosis due to increased metabolic oxygen demand and the production of lactic acid from cellular hypoxia at the injured site during the process of healing.[64] Studies also report that as wound healing begins, the natural physiological process tends to maintain the disturbed acidic milieu, restoring the pH balance by shifting from alkaline to acidic conditions. The acidic microenvironment is essential to maintain the appropriate oxygenation level required for fibroblast proliferation and collagen synthesis.[65] The release of CaP at this acidic wound microenvironment promotes fibroblast proliferation, induces blood clotting, and exerts a wound contraction effect on the wounds, thereby accelerating the wound healing process. Additionally, the release of calcium activates downstream molecules that play an important role in wound healing. At low concentrations, Ca^{2+} ions help in keratinocyte proliferation. On the other hand, at higher concentrations they facilitate keratinocyte differentiation, both of which are crucial for wound closure.[66]

3.11. Hemolysis assessment

The haemostatic phase is one of the primary and important stages in wound healing, in which the blood-clotting cascade gets initiated in order to prevent blood loss from the injured site, aiding in the wound healing process.[67] Scaffolds designed for wound healing application have direct contact with blood and blood components; hence, they should be hemocompatible and avoid adverse effects or destruction of the blood components.[68] According to the ASTM F756-00 protocol, a material is categorized as non-hemolytic if the hemolysis index of the material is between 0 and 2%.[69] Hemolysis studies were carried out on both CH-CA scaffolds and calcium-loaded CH-CA scaffolds at various concentrations (0.08 to 1.2 mg

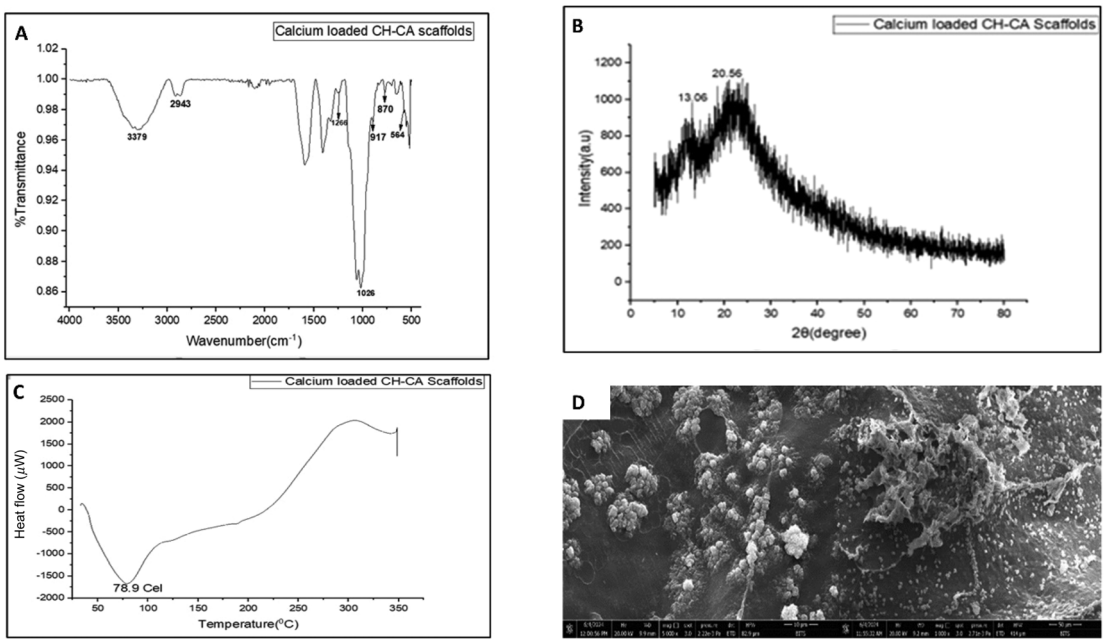

Fig. 7 (A) FTIR, (B) XRD, (C) DSC, and (D) SEM images of calcium-loaded CH-CA scaffolds.

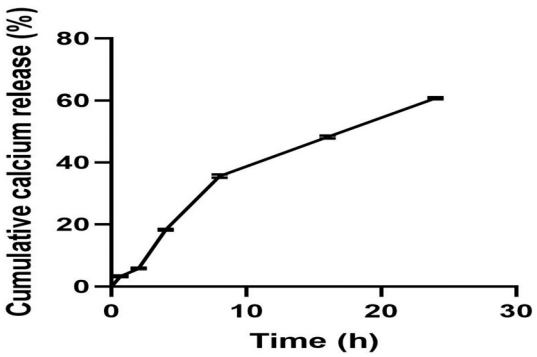

Fig. 8 *In vitro* calcium ion release study from CH-CA scaffolds.

mL^{-1}). Maximum hemolysis was observed at 1.2 mg mL^{-1}, which was 1.97 ± 0.11% and 1.11 ± 0.04% for CH-CA scaffolds and calcium-loaded CH-CA scaffolds, respectively (Fig. 9A and B). CH, being a cationic polymer, is widely used for its wound repair properties owing to its biocompatibility, biodegradability, hemostatic, and antimicrobial properties.[70] However, CA, an anionic polymer, due to its sulfate content is known to exert cytoprotective, anticoagulant, and immunomodulatory properties. Combination of these two polymers through electrostatic interaction during the formation of a PEC resulted in the formation of a composite material with enhanced biocompatibility and reduced cytotoxicity.[16] Additionally, the interaction resulted in the formation of a mesoporous structure which displayed higher blood cell attachment and platelet aggregation without any cytotoxicity. Similar results were observed in this study where the CH-CA scaffold exhibited excellent hemostatic activity against traumatic haemorrhage with enhanced tissue regeneration for wound healing.

Furthermore, upon loading calcium on the CH-CA scaffolds, there was a further reduction in %hemolysis, as calcium ions are known to be involved in various physiological processes aimed at maintaining the structural integrity of RBCs.[71] Finally, it can be concluded that the prepared scaffolds were hemocompatible and suitable for use in wound healing applications.

3.12. Protein adsorption studies

Protein adsorption studies are important in the case of scaffolds used for wound healing applications as these proteins play a significant role in hemostasis. Adsorbed proteins can enhance the biocompatibility of scaffolds by providing an interface between the scaffold and the biological environment; furthermore, it will promote cell adhesion and proliferation.[72]

According to Sharma S *et al.*, as the surface hydrophilicity of the scaffolds increases, an immediate 2-D layer forms between the scaffold and proteins. Afterward, protein molecules rapidly adsorb on this surface and form a new 3-D layer, further aiding in thrombosis formation.[26] This further plays a significant role in the wound-healing process.[72] The CH-CA scaffolds showed 5.55 ± 0.32 mg g^{-1} and calcium-loaded CH-CA scaffolds showed 15.64 ± 0.30 mg g^{-1} protein adsorption (Fig. 10). Calcium-loaded CH-CA scaffolds showed higher protein adsorption than CH-CA scaffolds. This protein adsorption ability can be correlated with the water absorption capacity and hydration of the scaffolds. The significant hydration and swelling in aqueous media shown by CH-CA scaffolds indicate their protein adsorption potential.[26] Another reason contributing to protein adsorption is the charge present on the polymers. According to Yadav P *et al.*, certain protonated amino groups present in CH at physiological pH may interact with the negative charges in proteins like BSA.[73] Calcium-loaded CH-CA scaffolds showed a higher protein

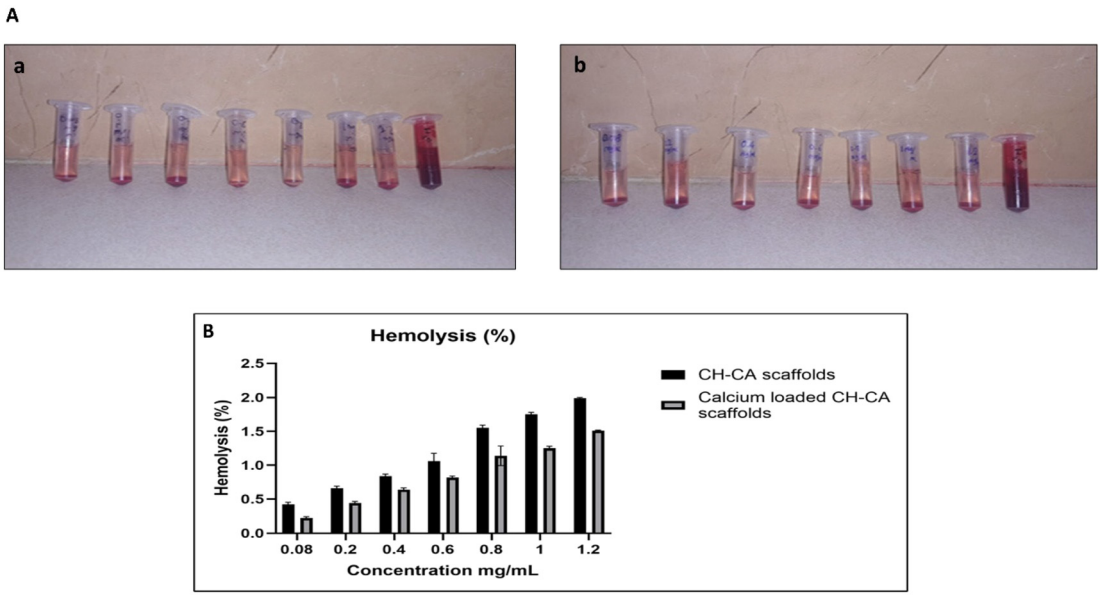

Fig. 9 (A) Pictorial representation of %hemolysis studies of (a) CH-CA scaffolds and (b) calcium loaded CH-CA scaffolds. (B) Graphical representation of %hemolysis studies of CH-CA scaffolds and calcium loaded CH-CA scaffolds.

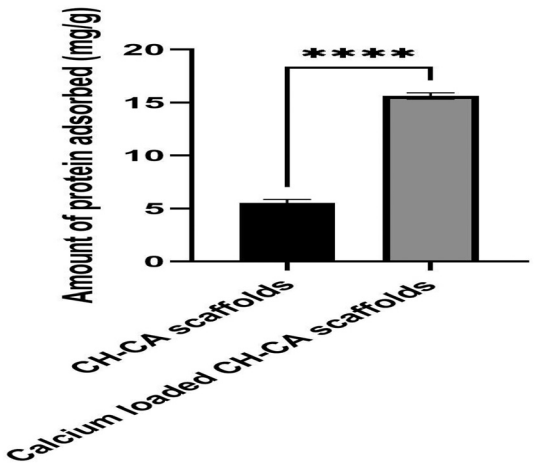

Fig. 10 Protein adsorption studies of CH-CA scaffolds and calcium-loaded CH-CA scaffolds. Data are shown as mean ± SD (****p < 0.0001).

adsorption value than CH-CA scaffolds. As per Nga NK *et al.*, various modifications can take place in the surface charges, surface morphology, chemical composition, and hydrophilicity after the incorporation of CaP in the scaffolds, leading to an increase in sites that can react with the proteins.[72]

3.13. *In ovo* angiogenesis activity analyzed using a chick yolk sac (YSM) assay

Angiogenesis is one of the prominent steps in the wound repair process. Newly formed blood vessels deliver oxygen and other essential nutrients, which fulfils the metabolic demand in various stages of wound healing and removes metabolic waste. Angiogenesis promotes the migration of various cells, including leucocytes, fibroblasts, and endothelial cells, which further facilitate the formation of the ECM, which further aids in the remodelling of the newly formed tissue.[74] The results from the angiogenesis study, observed after incubating eggs for 48 h with both CH-CA and calcium-loaded CH-CA scaffolds, showed significant growth of blood vessels. The formation of the CH-CA PEC created a synergistic effect in improving the overall performance of the scaffolds in terms of their biocompatibility. It provided a conducive hydrophilic environment to support cell proliferation and growth. Additionally, the composite PEC scaffold provided a porous structure, mimicking the natural ECM, thereby facilitating the infiltration of endothelial cells required for blood vessel formation. Furthermore, CH is known to stimulate the secretion of various growth factors such as the endothelial growth factor and fibroblast growth factor, supporting angiogenesis.[75]

The addition of calcium phosphate further enhanced the process of angiogenesis, as it promotes the activity of the vascular endothelial growth factor (VEGF), known to drive the process of angiogenesis. Xiu J *et al.* reported that combining fibrin glue with calcium phosphate cement for intramuscular implantation improved revascularization in rabbits.[76] Our study results concluded that both CH-CA scaffolds and calcium-loaded CH-CA scaffolds have angiogenic potential, further promoting the wound healing process. Fig. 11 demon-

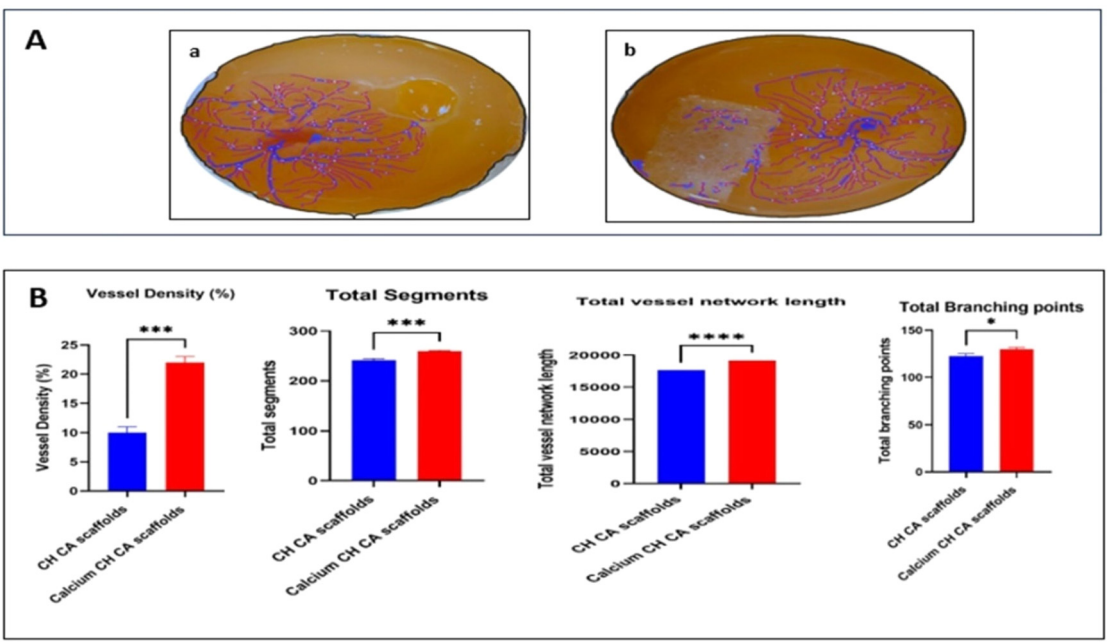

Fig. 11 (A) Assessment of the angiogenic potential of (a) calcium loaded CH-CA scaffolds and (b) CH-CA scaffolds. (B) Original and analyzed images of the yolk sac membrane assay obtained using the Wim CAM online tool (Wimasis) for quantitative assessment of the angiogenic potential in terms of vessel density, total branching points, total segments, and total vessel network length. Data are shown as mean ± SD (***P < 0.001, ****P < 0.0001, *P < 0.05).

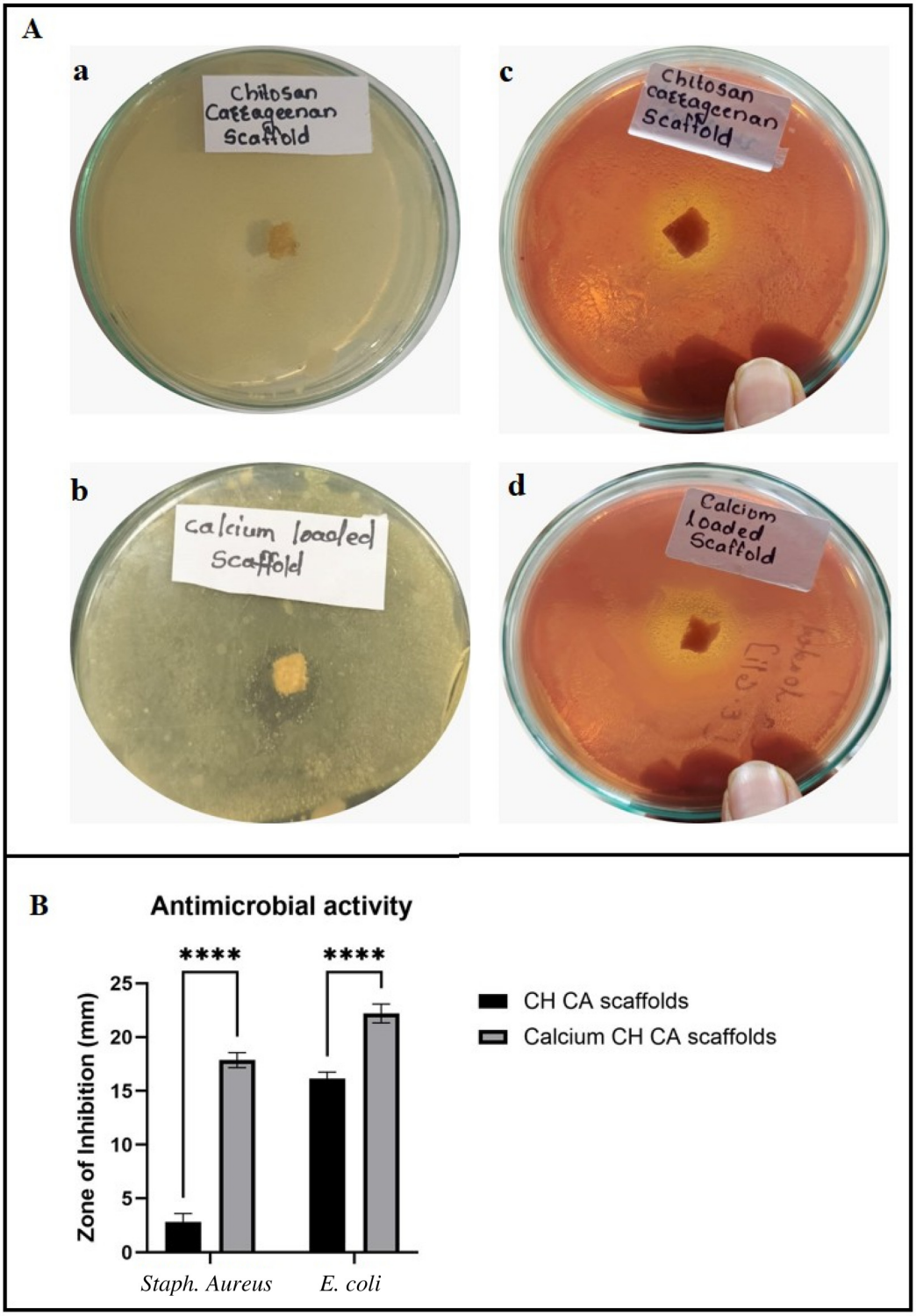

Fig. 12 (A) Antibacterial activity of (a) CH-CA scaffolds against *S. aureus*, (b) calcium-loaded CH-CA scaffolds against *S. aureus*, (c) CH-CA scaffolds against *E. coli*, and (d) calcium-loaded CH-CA scaffolds against *E. coli*. (B) Assessment of antibacterial activity of CH-CA scaffolds against *S. aureus* and *E. coli*.

strates that calcium-loaded CH-CA scaffolds show a significant increase in total vessel network length, vessel density, total segments, and total branching points compared to CH-CA scaffolds, indicating that calcium-loaded CH-CA scaffolds have angiogenic potential.

3.14. *In vitro* antimicrobial activity

Antimicrobial studies are crucial for scaffolds designed for wound healing purposes. Microbial colonization and biofilm formation may delay and further complicate the wound-healing process. The fabricated scaffolds should possess antimicrobial properties to prevent infections associated with microbial growth.[77] The antibacterial properties of CH-CA scaffolds and calcium-loaded CH-CA scaffolds were studied against *E. coli* and *S. aureus*. Results revealed that CH-CA scaffolds showed significant antibacterial activity against *E. coli*, and calcium-loaded CH-CA scaffolds exhibited increased antibacterial activity against *E. coli* and *S. aureus* compared to CH-CA scaffolds (Fig. 12A and B).

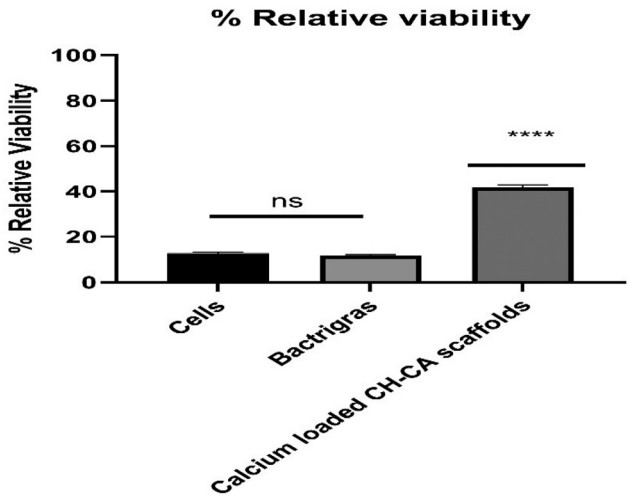

Fig. 13 The percentage relative viability of L929 cells seeded on the calcium-loaded CH-CA scaffolds at 24 h of culture. Data shown are mean ± SD (****p <0.0001, n = 3).

Several studies have demonstrated that carrageenan shows limited antibacterial activity. However, when combined with CH, it exhibited excellent antibacterial activity against *E. coli* due to the presence of CH in the scaffolds. Numerous studies have confirmed that CH exhibits strong activity against *E. coli*. This is attributed to the positive charge on CH arising from the amino groups in its structure, which allows it to interact with the negatively charged constituents of the bacterial cell membrane, altering its permeability and causing disruption. Similar results were observed in the studies by Guarnieri A *et al.* and Yan D *et al.*[78,79] When calcium phosphate was incorporated into the scaffolds, the antibacterial activity was enhanced compared to that of CH-CA scaffolds. The reason for this might be the release of Ca^{2+} ions from CaP powder, which interact with negatively charged constituents of bacterial cell walls, increasing membrane permeability, creating reactive oxygen species (ROS), and resulting in microbial cell lysis.[80]

3.15. MTT/cell proliferation assay

To evaluate the cytotoxicity of the scaffolds (calcium-loaded CH-CA), an MTT assay was used, which is a standard method for the early evaluation of biological materials for their therapeutic use. The results of the study indicated that the leachate from the scaffold did not affect cell viability, as shown in Fig. 13. After 24 hours, the calcium-loaded CH-CA scaffold significantly enhanced the percentage of relative cell viability in L929 cells (41.84%), showing an approximately 4.6-fold increase compared to both the cell-only control and the Bactigras-treated group. The study concluded the non-toxic nature of the scaffolds, proving that CH-CA and calcium phosphate powder are safe materials that can be used in combination to prepare polyelectrolyte complexes of CH and CA, loaded with calcium phosphate. The MTT assay confirmed the biocompatibility of the scaffolds through evaluating metabolic activity and cell viability. The assay results confirmed the ability of scaffolds to promote cell viability and support normal cellular proliferation and migration without impairing cellular functions. The cells treated with the scaffolds exhibited a higher cell proliferation rate without affecting the cellular

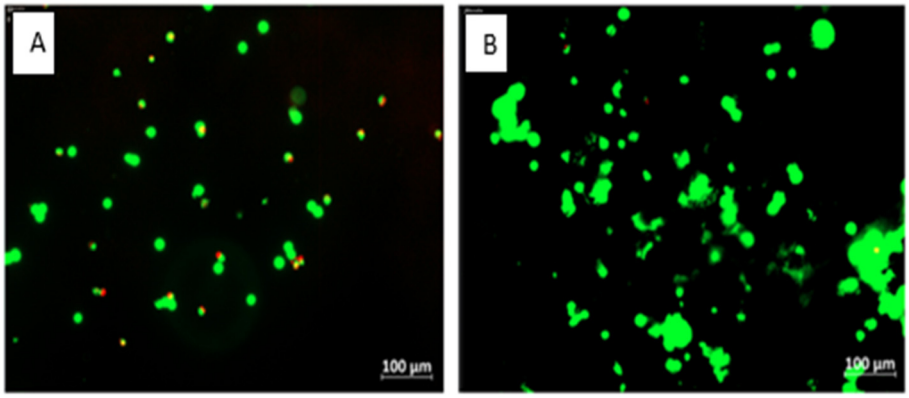

Fig. 14 Live/dead images of L929 cells seeded on (A) Bactigras and (B) calcium-loaded CH-CA scaffolds at 48 h of culture.

morphology. The developed calcium-loaded (CH-CA) scaffolds demonstrated a favourable impact on the proliferation of L929 mouse fibroblast cells, thereby providing evidence for the safety and biocompatibility of the scaffolds for wound healing applications.

3.16. Live/dead assay

The cell viability was further evaluated by a live/dead assay, as shown in Fig. 14. This assay provides crucial information on cellular function and differentiates between live/dead cells based on their metabolic activity and their membrane integrity.[81,82] The calcium-loaded CH-CA scaffolds displayed a significant rise in cell viability compared to the marketed sample. CH has adhesive properties that promote attachment, facilitating cell–substrate contact and proliferation.[83] Additionally, it has bioactive properties that create a favourable environment for cell proliferation. CA is known to possess excellent water retention ability, which helps maintain a moist environment for cell attachment and proliferation.[16] The SEM studies revealed the porous structure of the CH-CA scaffolds, which further assisted in cell attachment and infiltration. The interconnected porous structure mimics the ECM, allowing cell-to-cell communication, providing space for survival and attachment, and facilitating nutrient exchange, which further promotes cell growth or proliferation.[83] Calcium ions are important secondary messengers in intracellular signalling, activating various signalling pathways during wound healing, which promotes cell proliferation and differentiation. Calcium is known to facilitate fibroblastic differentiation, aiding in the wound-healing process.[5] The study concluded that the combination of CH, CA, and CaP exhibited a synergistic effect, promoting cell proliferation and improving cell viability, as shown in Fig. 14.

4. Conclusion

In this study, scaffolds were prepared by a polyelectrolyte complexation method using CH as a cationic polymer with anionic polymers like PE, SA, and CA *via* the lyophilization process. The PEC formation was confirmed by FTIR, XRD, and DSC. CH-CA scaffolds exhibited better swelling, porosity, and degradation; hence, they were used to load calcium phosphate. Calcium phosphate was synthesized by microwave-assisted synthesis, which is considered a green synthetic route. Calcium-loaded CH-CA scaffolds released 60.75% Ca^{+} ions from the scaffolds in the acidic environment of the wound area at a controlled rate for a period of 24 h. The scaffolds exhibited good antimicrobial activity against both *S. aureus* and *E. coli*. Additionally, the scaffolds displayed angiogenic potential by promoting the development of new blood vessels and demonstrated significant hemocompatibility with <2% hemolysis (at concentrations from 0.08 to 1.2 mg mL^{-1}). The study revealed a significant protein adsorption capacity of the scaffolds compared to CH-CA scaffolds. The *in vitro* cytotoxicity study revealed a significant increase in the cell density of the L929 mouse fibroblast cell line cultures, indicating their potential to stimulate cell growth and support tissue regeneration for accelerated wound healing. The study provides a simple yet effective approach for wound management using calcium phosphate-loaded CH-CA scaffolds and indicates their potential to be developed as a wound dressing material.

Author contributions

Vinita Patole: writing – original draft, writing – review & editing, methodology, investigation, conceptualization. Gaurav Kavitkar: writing – original draft, methodology, formal analysis. Ganesh Ingavle: supervision, methodology, formal analysis. Isha Behere: writing – original draft, methodology, formal analysis. Ravindra Wavhale: methodology, investigation, formal analysis. Avinash Sanap: writing – review & editing, methodology, data curation. Abhishek Jha: formal analysis, data curation, writing – review & editing. Sanjeevani Deshkar: methodology, formal analysis. Pramod Sakpal: methodology, formal analysis.

Data availability

The authors confirm that the data supporting the finding of this study are available within the article.

Conflicts of interest

There are no conflicts to declare.

Acknowledgements

We would like to thank Dr Vaijayanti Kale, Head and Professor, Symbiosis Centre for Stem Cell Research (SCSCR), Symbiosis International (Deemed University), Pune, India, for sharing the L929 mouse dermal fibroblast cells for cytotoxicity studies. The authors would also like to thank Dr Divya Ottoor, Associate Professor, Department of Chemistry, Savitribai Phule Pune University, and Ms. Nikita Vywahare PhD Scholar, Department of Chemistry, Savitribai Phule Pune University, for assisting in carrying out the FTIR and XRD analyses.

References

1 M. Abazari, A. Ghaffari, H. Rashidzadeh, S. M. Badeleh and Y. A. Maleki, systematic review on classification, identification, and healing process of burn wound healing, *Int. J. Lower Extremity Wounds*, 2022, **21**(1), 18–30.
2 C. Tyavambiza, M. Meyer and S. Meyer, Cellular and molecular events of wound healing and the potential of silver based nanoformulations as wound healing agents, *Bioengineering*, 2022, **9**(11), 712.

3 H. N. Wilkinson and M. J. Hardman, Wound healing: cellular mechanisms and pathological outcomes, *Open Biol.*, 2020, **10**(9), 200223.
4 S. J. Ghilardi, B. M. O'Reilly and A. E. Sgro, Intracellular signaling dynamics and their role in coordinating tissue repair, *Wiley Interdiscip. Rev.:Syst. Biol. Med.*, 2020, **12**(3), 1479.
5 T. Subramaniam, M. B. Fauzi, Y. Lokanathan and J. X. Law, The role of calcium in wound healing, *Int. J. Mol. Sci.*, 2021, **22**(12), 6486.
6 M. Mussbacher, J. B. Kral-Pointner, M. Salzmann, W. C. Schrottmaier and A. Assinger, Mechanisms of hemostasis: Contributions of platelets, coagulation factors, and the vessel wall, in *Fundamentals of Vascular Biology*, 2024, pp. 167–203.
7 F. Moccia, S. Negri, M. Shekha, P. Faris and G. Guerra, Endothelial Ca^{2+} signaling, angiogenesis and vasculogenesis: just what it takes to make a blood vessel, *Int. J. Mol. Sci.*, 2019, **20**(16), 3962.
8 W. E. Müller, H. Schepler, M. Neufurth, S. Wang, V. Ferrucci, M. Zollo, R. Tan, H. C. Schröder and X. Wang, The physiological polyphosphate as a healing biomaterial for chronic wounds: Crucial roles of its antibacterial and unique metabolic energy supplying properties, *J. Mater. Sci. Technol.*, 2023, **135**, 170–185.
9 A. Patil, S. Nangare, P. Mahajan, P. Jain and L. Zawar, Chitosan and neem gum-based polyelectrolyte complex for design of allantoin loaded biocomposite film: *In vitro*, *ex vivo*, and *in vivo* characterization, *Int. J. Biol. Macromol.*, 2024, **263**, 130280.
10 G. Satchanska, S. Davidova and P. D. Petrov, Natural and Synthetic Polymers for Biomedical and Environmental Applications, *Polymers*, 2024, **16**(8), 1159.
11 D. S. Rajkumar, K. Keerthika and V. Vijayaragavan, Chitosan-Based Biomaterial in Wound Healing: A Review, *Cureus*, 2024, **16**(2), 55193.
12 J. Radwan-Pragłowska, M. Piątkowski, V. Deineka, Ł. Janus, V. Korniienko, E. Husak, V. Holubnycha, I. Liubchak, V. Zhurba, A. Sierakowska and M. Pogorielov, Chitosan-based bioactive hemostatic agents with antibacterial properties—synthesis and characterization, *Molecules*, 2019, **24**(14), 2629.
13 G. Yaşayan, Chitosan films and chitosan/pectin polyelectrolyte complexes encapsulating silver sulfadiazine for wound healing, *Istanbul J. Pharm.*, 2020, **50**(3), 238–244.
14 S. Alven and B. A. Aderibigbe, Chitosan-Based Scaffolds Incorporated with Silver Nanoparticles for the Treatment of Infected Wounds, *Pharmaceutics*, 2024, **16**(3), 327.
15 N. N. Nordin, N. K. Aziz, I. Naharudin and N. K. Anuar, Effects of Drug-Free Pectin Hydrogel Films on Thermal Burn Wounds in Streptozotocin-Induced Diabetic Rats, *Polymers*, 2022, **14**(14), 2873.
16 B. Neamtu, A. Barbu, M. O. Negrea, C.Ş. Berghea-Neamțu, D. Popescu, M. Zăhan and V. Mireşan, Carrageenan-based compounds as wound healing materials, *Int. J. Mol. Sci.*, 2022, **23**(16), 9117.
17 S. Ulagesan, S. Krishnan, T. J. Nam and Y. H. Choi, The influence of κ-carrageenan-R-phycoerythrin hydrogel on in vitro wound healing and biological function, *Int. J. Mol. Sci.*, 2023, **24**(15), 12358.
18 R. A. Raus, W. M. F. W. Nawawi and R. R. Nasaruddin, Alginate and alginate composites for biomedical applications, *Asian J. Pharm. Sci.*, 2021, **16**(3), 280–306.
19 B. Ishfaq, I. U. Khan, S. H. Khalid and S. Asghar, Design and evaluation of sodium alginate-based hydrogel dressings containing Betula utilis extract for cutaneous wound healing, *Front. Bioeng. Biotechnol.*, 2023, **11**, 1042077.
20 S. Deshkar, P. Yeole, J. Mahore, A. Shinde and P. Giram, Polyelectrolyte-Complex-Based Hydrogel Inserts for Vaginal Delivery of Posaconazole and Probiotics, *Gels*, 2023, **9**(11), 851.
21 E. S. Dragan, M. V. Dinu and C. A. Ghiorghita, Chitosan-based polyelectrolyte complex cryogels with elasticity, toughness and delivery of curcumin engineered by polyions pair and cryostructuration steps, *Gels*, 2022, **8**(4), 240.
22 D. C. M. Ferreira, S. O. Ferreira, E. S. de Alvarenga, N. D. F. F. Soares, J. S. dos Reis Coimbra and E. B. de Oliveira, Polyelectrolyte complexes (PECs) obtained from chitosan and carboxymethylcellulose: A physicochemical and microstructural study, *Carbohydr. Polym. Technol. Appl.*, 2022, **3**, 100197.
23 I. Dogaris, I. Pylypchuk, G. Henriksson and A. Abbadess, Polyelectrolyte complexes based on a novel and sustainable hemicellulose-rich lignosulphonate for drug delivery applications, *Drug Delivery Transl. Res.*, 2024, **14**, 1–5.
24 F. S. Rezaei, A. Khorshidian, F. M. Beram, A. Derakhshani, J. Esmaeili and A. Barati, 3D printed chitosan/polycaprolactone scaffold for lung tissue engineering: hope to be useful for COVID-19 studies, *RSC Adv.*, 2021, **11**(32), 19508–19520.
25 A. Deng, Y. Yang and S. Du, Tissue engineering 3D porous scaffolds prepared from electrospun recombinant human collagen (RHC) polypeptides/chitosan nanofibers, *Appl. Sci.*, 2021, **11**(11), 5096.
26 S. Sharma, K. L. Swetha and A. Roy, Chitosan-Chondroitin sulfate based polyelectrolyte complex for effective management of chronic wounds, *Int. J. Biol. Macromol.*, 2019, **132**, 97–108.
27 A. E. Italiano, R. L. Tranquilin, D. O. Marin, M. L. Santos and L. G. Vaz, Synthesis of Calcium Phosphate by Microwave Hydrothermal Method: Physicochemical and Morphological Characterization, *Int. J. Biomater.*, 2024, **2024**(1), 2167066.
28 M. G. Pilgrim, S. Marouf, S. Fearn, L. Csincsik, E. Kortvely, J. C. Knowles, G. Malek, R. B. Thompson and I. Lengyel, Characterization of calcium phosphate spherical particles in the subretinal pigment epithelium–basal lamina space in aged human eyes, *Ophthalmol. Sci.*, 2021, **1**(3), 100053.
29 S. Hesaraki, G. Saba, M. Shahrezaee, N. Nezafati, Z. Orshesh, F. Roshanfar, S. Borhan, B. Glasmacher, P. Makvandi and Y. Xu, Reinforcing β-tricalcium phosphate scaffolds for potential applications in bone tissue engineer-

ing: impact of functionalized multi-walled carbon nanotubes, *Sci. Rep.*, 2024, **14**(1), 19055.

30 M. A. Rahman, M. S. Islam, P. Haque, M. N. Khan, M. Takafuji, M. Begum, G. W. Chowdhury, M. Khan and M. M. Rahman, Calcium ion mediated rapid wound healing by nano-ZnO doped calcium phosphate-chitosan-alginate biocomposites, *Materialia*, 2020, **13**, 00839.

31 N. Golafshan, R. Rezahasani, M. T. Esfahani, M. Kharaziha and S. N. Khorasani, Nanohybrid hydrogels of laponite: PVA-Alginate as a potential wound healing material, *Carbohydr. Polym.*, 2017, **176**, 392–401.

32 A. S. Neto, P. Pereira, A. C. Fonseca, C. Dias, M. C. Almeida, I. Barros, C. O. Miranda, L. P. de Almeida, P. V. Morais, J. F. Coelho and J. M. Ferreira, Highly porous composite scaffolds endowed with antibacterial activity for multifunctional grafts in bone repair, *Polymers*, 2021, **13**(24), 4378.

33 D. C. Kennedy, B. Coen, A. M. Wheatley and K. J. McCullagh, Microvascular experimentation in the chick chorioallantoic membrane as a model for screening angiogenic agents including from gene-modified cells, *Int. J. Mol. Sci.*, 2021, **23**(1), 452.

34 V. Patole, P. Bhosale, G. Ingavle, I. Behere, N. Vyawahare, D. Ottoor, A. Sanap, R. Bhonde and S. Kheur, In vitro and in vivo assessment of gallic acid-chitosan/polycaprolactone conjugate electrospun nanofibers for wound healing, *J. Drug Delivery Technol.*, 2024, **95**, 105569.

35 M. R. Shekatkar, S. M. Kheur, A. H. Kharat, S. S. Deshpande, A. P. Sanap, M. G. Kheur and R. R. Bhonde, Assessment of angiogenic potential of mesenchymal stem cells derived conditioned medium from various oral sources, *J. Clin. Transl. Res.*, 2022, **8**(4), 323.

36 P. Sugeena and S. Tharalakshmi, Cytotoxicity evaluation of Swasanandam Gutika by MTT assay in mouse fibroblast cells, *Int. J. Health Sci. Res.*, 2020, **10**(6), 30–35.

37 V. N. Davydova, N. V. Krylova, O. V. Iunikhina, A. V. Volod'ko, E. A. Pimenova, M. Y. Shchelkanov and I. M. Yermak, Physicochemical properties and antiherpetic activity of κ-carrageenan complex with chitosan, *Mar. Drugs*, 2023, **21**(4), 238.

38 J. Qian, Y. Chen, Q. Wang, X. Zhao, H. Yang, F. Gong and H. Guo, Preparation and antimicrobial activity of pectin-chitosan embedding nisin microcapsules, *Eur. Polym. J.*, 2021, **157**, 110676.

39 X. B. Yin, Q. Z. Yu, B. W. Li and C. D. Zhang, Preparation and characterization of sodium alginate/chitosan composite nanoparticles loaded with chondroitin sulfate, *Adv. Mater. Sci. Eng.*, 2021, **2021**(1), 6665488.

40 A. M. Hezma, W. A. Shaltout, H. A. Kabary, G. S. El-Bahy and A. B. Abdelrazzak, Fabrication, characterization and adsorption investigation of Nano zinc oxide–sodium alginate beads for effective removal of chromium(VI) from aqueous solution, *J. Inorg. Organomet. Polym. Mater.*, 2023, **33**(5), 1400–1408.

41 K. M. Wani and R. V. Uppaluri, Characterization of pectin extracted from pomelo peel using pulsed ultrasound assisted extraction and acidic hot water extraction process, *Appl. Food Res.*, 2023, **3**(2), 100345.

42 R. Chitra, P. Sathya, S. Selvasekarapandian, S. Monisha, V. Moniha and S. Meyvel, Synthesis and characterization of iota-carrageenan solid biopolymer electrolytes for electrochemical applications, *Ionics*, 2019, **25**(5), 2147–2157.

43 S. G. Fisher, H. C. Chiang, E. T. Iverson, E. Chang and J. C. Grunlan, Hydrogen bonded polymer complex thin films for highly stretchable gas barriers, *RSC Appl. Polym.*, 2024, **2**(3), 356–364.

44 L. Rahman, J. Goswami and D. Choudhury, Assessment of physical and thermal behaviour of chitosan-based biocomposites reinforced with leaf and stem extract of Tectona grandis, *Polym. Compos.*, 2022, **30**, 09673911221076305.

45 H. E. Gültekin, M. İlhan and F. Nalbantoğlu, A new approach to oral dosage forms: carrageenan-based vegan gummies, *J. Pharm. Res.*, 2024, **28**, 225–235.

46 J. A. Sánchez-Fernández, G. Presbítero-Espinosa, L. Peña-Parás, E. I. Pizaña, K. P. Galván, M. Vopálenský, I. Kumpová and L. E. Elizalde-Herrera, Characterization of sodium alginate hydrogels reinforced with nanoparticles of hydroxyapatite for biomedical applications, *Polymers*, 2021, **13**(17), 2927.

47 S. Braccini, C. B. Chen, J. J. Łucejko, F. Barsotti, C. Ferrario, G. Q. Chen and D. Puppi, Additive manufacturing of wet-spun chitosan/hyaluronic acid scaffolds for biomedical applications, *Carbohydr. Polym.*, 2024, **329**, 121788.

48 J. Potaś, E. Szymańska, M. Wróblewska, I. Kurowska, M. Maciejczyk, A. Basa, E. Wolska, A. Z. Wilczewska and K. Winnicka, Multilayer films based on chitosan/pectin polyelectrolyte complexes as novel platforms for buccal administration of clotrimazole, *Pharmaceutics*, 2021, **13**(10), 1588.

49 N. E. Beltran-Vargas, E. Peña-Mercado, C. Sánchez-Gómez, M. Garcia-Lorenzana, J. C. Ruiz, I. Arroyo-Maya, S. Huerta-Yepez and J. Campos-Terán, Sodium alginate/chitosan scaffolds for cardiac tissue engineering: The influence of its three-dimensional material preparation and the use of gold nanoparticles, *Polymers*, 2022, **14**(16), 3233.

50 Y. D. Nokoorani, A. Shamloo, M. Bahadoran and H. Moravvej, Fabrication and characterization of scaffolds containing different amounts of allantoin for skin tissue engineering, *Sci. Rep.*, 2021, **11**(1), 16164.

51 K. Nuutila and E. Eriksson, Moist wound healing with commonly available dressings, *Adv. Wound Care*, 2021, **10**(12), 685–698.

52 T. L. D. A. Montanheiro, L. S. Montagna, V. Patrulea, O. Jordan, G. Borchard, G. M. M. Lobato, L. H. Catalani and A. P. Lemes, Evaluation of cellulose nanocrystal addition on morphology, compression modulus and cytotoxicity of poly (3-hydroxybutyrate-co-3-hydroxyvalerate) scaffolds, *J. Mater. Sci.*, 2019, **54**, 7198–7210.

53 H. Nosrati, R. Aramideh Khouy, A. Nosrati, M. Khodaei, M. Banitalebi-Dehkordi, K. Ashrafi-Dehkordi, S. Sanami and Z. Alizadeh, Nanocomposite scaffolds for accelerating

chronic wound healing by enhancing angiogenesis, *J. Nanobiotechnol.*, 2021, **19**, 1–21.

54 M. C. Bonferoni, C. Caramella, L. Catenacci, B. Conti, R. Dorati, F. Ferrari, I. Genta, T. Modena, S. Perteghella, S. Rossi and G. Sandri, Biomaterials for soft tissue repair and regeneration: A focus on italian research in the field, *Pharmaceutics*, 2021, **13**(9), 1341.

55 A. I. Visan, G. Popescu-Pelin and G. Socol, Degradation behavior of polymers used as coating materials for drug delivery—A basic review, *Polymers*, 2021, **13**(8), 1272.

56 M. Espanol, E. Davis, E. Meslet, G. Mestres, E. B. Montufar and M. P. Ginebra, Effect of moisture on the reactivity of alpha-tricalcium phosphate, *Ceram. Int.*, 2023, **49**(11), 18228–18237.

57 M. Henary, C. Kananda, L. Rotolo, B. Savino, E. A. Owens and G. Cravotto, Benefits and applications of microwave-assisted synthesis of nitrogen containing heterocycles in medicinal chemistry, *RSC Adv.*, 2020, **10**(24), 14170–14197.

58 E. Gabano and M. Ravera, Microwave-Assisted Synthesis: Can Transition Metal Complexes Take Advantage of This "Green" Method?, *Molecules*, 2022, **27**(13), 4249.

59 M. S. Hossain and S. Ahmed, FTIR spectrum analysis to predict the crystalline and amorphous phases of hydroxyapatite: a comparison of vibrational motion to reflection, *RSC Adv.*, 2023, **13**(21), 14625–14630.

60 A. Indurkar, R. Choudhary, K. Rubenis, M. Nimbalkar, A. Sarakovskis, A. R. Boccaccini and J. Locs, Amorphous calcium phosphate and amorphous calcium phosphate carboxylate: synthesis and characterization, *ACS Omega*, 2023, **8**(30), 26782–26792.

61 T. H. A. Corrêa and J. N. F. Holanda, Fish bone as a source of raw material for synthesis of calcium phosphate, *Mater. Res.*, 2019, **22**, 20190486.

62 N. Tan, M. Sabalic-Schoener, L. Nguyen and F. D'Aiuto, β-Tricalcium phosphate-loaded chitosan-based thermosensitive hydrogel for periodontal regeneration, *Polymers*, 2023, **15**(20), 4146.

63 W. A. Al-Masry, S. Haider, A. Mahmood, M. Khan, S. F. Adil and M. R. Siddiqui, Evaluation of the thermal and morphological properties of γ-irradiated chitosan-glycerol-based polymeric films, *Processes*, 2021, **9**(10), 1783.

64 S. Wang, M. Neufurth, H. Schepler, R. Tan, Z. She, B. Al-Nawas, X. Wang, H. C. Schröder and W. E. Müller, Acceleration of wound healing through amorphous calcium carbonate, stabilized with high-energy polyphosphate, *Pharmaceutics*, 2023, **15**(2), 494.

65 P. Sim, X. L. Strudwick, Y. Song, A. J. Cowin and S. Garg, Influence of acidic pH on wound healing in vivo: a novel perspective for wound treatment, *Int. J. Mol. Sci.*, 2022, **23**(21), 13655.

66 O. Krizanova, A. Penesova, J. Sokol, A. Hokynkova, A. Samadian and P. Babula, Signaling pathways in cutaneous wound healing, *Front. Physiol.*, 2022, **13**, 1030851.

67 H. Wang and L. Yang, Applications of injectable hemostatic materials in wound healing: principles, strategies, performance requirements, and future perspectives, *Theranostics*, 2023, **13**(13), 4615.

68 P. Yu and W. Zhong, Hemostatic materials in wound care, *Burns Trauma*, 2021, **9**, 019.

69 B. Kaczmarek, O. Mazur, O. Miłek, M. Michalska-Sionkowska, A. Das, A. Jaiswal, J. Vishnu, K. Tiwari, A. Sionkowska, A. M. Osyczka and G. Manivasagam, Design, characterization and in vitro evaluation of thin films enriched by tannic acid complexed by Fe(III) ions, *Prog. Biomater.*, 2020, **9**, 249–257.

70 C. López-Iglesias, J. Barros, I. Ardao, F. J. Monteiro, C. Alvarez-Lorenzo, J. L. Gómez-Amoza and C. A. García-González, Vancomycin-loaded chitosan aerogel particles for chronic wound applications, *Carbohydr. Polym.*, 2019, **204**, 223–231.

71 L. Kaestner, A. Bogdanova and S. Egee, Calcium channels and calcium-regulated channels in human red blood cells, *Calcium Signaling*, 2020, 625–648.

72 N. K. Nga, L. T. T. Tam, N. T. Ha, P. H. Viet and T. Q. Huy, Enhanced biomineralization and protein adsorption capacity of 3D chitosan/hydroxyapatite biomimetic scaffolds applied for bone-tissue engineering, *RSC Adv.*, 2020, **10**(70), 43045–43057.

73 P. Yadav and A. B. Yadav, Preparation and characterization of BSA as a model protein loaded chitosan nanoparticles for the development of protein-/peptide-based drug delivery system, *Future J. Pharm. Sci.*, 2021, **7**, 1–9.

74 P. A. Everts, J. F. Lana, K. Onishi, D. Buford, J. Peng, A. Mahmood, L. F. Fonseca, A. van Zundert and L. Podesta, Angiogenesis and tissue repair depend on platelet dosing and bioformulation strategies following orthobiological platelet-rich plasma procedures: a narrative review, *Biomedicines*, 2023, **11**(7), 1922.

75 N. Lv, Z. Zhou, M. Hou, L. Hong, H. Li, Z. Qian, X. Gao and M. Liu, Research progress of vascularization strategies of tissue-engineered bone, *Front. Bioeng. Biotechnol.*, 2024, **11**, 1291969.

76 X. Jiang, J. Wang, X. Deng, F. Xiong, S. Zhang, Z. Gong, X. Li, K. Cao, H. Deng, Y. He and Q. Liao, The role of microenvironment in tumor angiogenesis, *J. Exp. Clin. Cancer Res.*, 2020, **39**, 1–9.

77 G. R. Jiménez-Gastélum, E. M. Aguilar-Medina, E. Soto-Sainz, R. Ramos-Payán and E. L. Silva-Benítez, Antimicrobial properties of extracellular matrix scaffolds for tissue engineering, *Biomed Res. Int.*, 2019, **2019**(1), 9641456.

78 A. Guarnieri, M. Triunfo, C. Scieuzo, D. Ianniciello, E. Tafi, T. Hahn, S. Zibek, R. Salvia, A. De Bonis and P. Falabella, Antimicrobial properties of chitosan from different developmental stages of the bioconverter insect Hermetia illucens, *Sci. Rep.*, 2022, **12**(1), 8084.

79 D. Yan, Y. Li, Y. Liu, N. Li, X. Zhang and C. Yan, Antimicrobial properties of chitosan and chitosan derivatives in the treatment of enteric infections, *Molecules*, 2021, **26**(23), 7136.

80 H. Elsawy, H. M. Abd El-Lateef, M. M. Khalaf, I. M. Mohamed, A. H. Touny and A. Toghan, Synthesis and

antimicrobial activity assessment of calcium and iron phosphate nanoparticles prepared by a facile and cost-effective method, *Chem. Phys. Lett.*, 2021, **779**, 138839.
81 W. Peng, T. Polajžer, C. Yao and D. Miklavčič, Dynamics of cell death due to electroporation using different pulse parameters as revealed by different viability assays, *Ann. Biomed. Eng.*, 2024, **52**(1), 22–35.
82 M. M. Islam, M. Shahruzzaman, S. Biswas, M. N. Sakib and T. U. Rashid, Chitosan based bioactive materials in tissue engineering applications-A review, *Bioact. Mater.*, 2020, **5**(1), 164–183.
83 O. Vesvoranan, A. Anup and K. R. Hixon, Current concepts and methods in tissue interface scaffold fabrication, *Biomimetics*, 2022, **7**(4), 151.